

Assessing functional connectivity across 3D tissue engineered axonal tracts using calcium fluorescence imaging

Anjali Vijay Dhobale¹, Dayo O Adewole^{2,3,4}, Andy Ho Wing Chan⁵,
Toma Marinov¹, Mijail D Serruya^{3,5}, Reuben H Kraft^{1,6,7} 
and D Kacy Cullen^{2,3,4,7}

¹ The Penn State Computational Biomechanics Group, The Pennsylvania State University, University Park, PA, United States of America

² Center for Brain Injury and Repair, Department of Neurosurgery, Perelman School of Medicine, University of Pennsylvania, Philadelphia, PA, United States of America

³ Center for Neurotrauma, Neurodegeneration and Restoration, Corporal Michael J. Crescenz Veterans Affairs Medical Center, Philadelphia, PA, United States of America

⁴ Department of Bioengineering, School of Engineering and Applied Science, University of Pennsylvania, Philadelphia, PA, United States of America

⁵ Department of Neurology and Sidney Kimmel Medical College, Thomas Jefferson University, Philadelphia, PA, United States of America

⁶ Department of Biomedical Engineering, The Pennsylvania State University, University Park, PA, United States of America

E-mail: reuben.kraft@psu.edu (R H Kraft) or dkacy@pennteam.upenn.edu (D Kacy Cullen)

Received 24 November 2017, revised 25 May 2018

Accepted for publication 1 June 2018

Published 11 July 2018



Abstract

Objective. Micro-tissue engineered neural networks (micro-TENNs) are anatomically-inspired constructs designed to structurally and functionally emulate white matter pathways in the brain. These 3D neural networks feature long axonal tracts spanning discrete neuronal populations contained within a tubular hydrogel, and are being developed to reconstruct damaged axonal pathways in the brain as well as to serve as physiologically-relevant *in vitro* experimental platforms. The goal of the current study was to characterize the functional properties of these neuronal and axonal networks. **Approach.** Bidirectional micro-TENNs were transduced to express genetically-encoded calcium indicators, and spontaneous fluorescence activity was recorded using real-time microscopy at 20 Hz from specific regions-of-interest in the neuronal populations. Network activity patterns and functional connectivity across the axonal tracts were then assessed using various techniques from statistics and information theory including Pearson cross-correlation, phase synchronization matrices, power spectral analysis, directed transfer function, and transfer entropy. **Main results.** Pearson cross-correlation, phase synchronization matrices, and power spectral analysis revealed high values of correlation and synchronicity between the spatially segregated neuronal clusters connected by axonal tracts. Specifically, phase synchronization revealed high synchronicity of >0.8 between micro-TENN regions of interest. Normalized directed transfer function and transfer entropy matrices suggested robust information flow between the neuronal populations. Time varying power spectrum analysis revealed the strength of information propagation at various frequencies. Signal power strength was visible at elevated peak levels for dominant delta (1–4 Hz) and theta (4–8 Hz) frequency bands and progressively weakened at higher frequencies. These signal power strength results closely matched normalized directed transfer

⁷ Co-senior authors.

function analysis where near synchronous information flow was detected between frequencies of 2–5 Hz. *Significance.* To our knowledge, this is the first report using directed transfer function and transfer entropy methods based on fluorescent calcium activity to estimate functional connectivity of distinct neuronal populations via long-projecting, 3D axonal tracts *in vitro*. These functional data will further improve the design and optimization of implantable neural networks that could ultimately be deployed to reconstruct the nervous system to treat neurological disease and injury.

Keywords: axonal tracts, functional connectivity, fluorescence calcium imaging, directed transfer function (DTF), transfer entropy (TE), engineered neural networks

(Some figures may appear in colour only in the online journal)

1. Introduction

Recent advancements in neural tissue engineering methodologies allow for the *in vitro* fabrication of more sophisticated three-dimensional (3D) constructs designed to replicate the structure and function of specialized neural networks in the brain [1–4]. Micro-tissue engineered neural networks (micro-TENNs) are living, 3D constructs consisting of discrete populations of neurons (i.e. aggregates with specified phenotype) spanned by aligned axonal tracts protected in a soft hydrogel cylinder (figure 1). These micro-TENNs reconstitute the architecture of long-distance axonal tracts in the brain, and are being developed for two complementary purposes: (1) to be transplanted *en masse* to integrate with targeted brain circuitry and thereby reconstruct and/or modulate damaged axonal pathways, and (2) to serve as biofidelic *in vitro* test-beds to study development, functionality, injury/disease responses, and/or pharmacologic strategies in an anatomically-relevant, yet controlled setting.

We have previously demonstrated potential applications of micro-TENNs to reconstruct long-distance white matter (i.e. axonal) pathways in the brain [1–4]. Further, we have recently begun to apply micro-TENNs as the first implantable ‘living electrodes’ designed to biologically integrate with deep host neurons while the other end remains quasi-externalized, thereby serving as the living component of a biohybrid neural interface with non-organic components relegated to the brain surface (figure 1(c)) [4, 5]. As ‘living electrodes’, we are exploring the capability of these neuron-based constructs to form stable synaptic connections in targeted cortical layers to selectively display a facsimile of deep brain activity to the cortical surface and/or provide a conduit to modulate host network activity upon stimulation of the dorsal neuronal aggregate within the micro-TENN. To realize this long-term goal, we have to first understand the underlying organizational connectivity patterns associated with micro-TENNs. This can be evaluated in two phases. In the first phase, which is the goal of the current study, we aim to characterize the functional attributes of fully formed micro-TENN neurons and axonal tracts *in vitro*. Specifically, we seek to characterize the activity patterns, degree of synchronization, and functional connectivity of micro-TENNs non-invasively (i.e. without penetrating the aggregates

with electrodes) based on real-time microscopy of spatial dynamics of calcium oscillations using GCaMP6, a genetically-encoded calcium indicator (GECI). This powerful method allows the acquisition of a spatial map of activity patterns both within the segregated neuronal populations as well as across the long axonal tracts connecting them, with sophisticated statistical and information theory methods then deployed to understand relationships between activity patterns and functional connectivity of these complex, 3D neuronal networks with long-projecting axonal tracts. In the second phase, to be completed in future work, we will characterize alterations in network activity and functional activity patterns following implantation and synaptic integration of micro-TENNs in the brain [1, 2].

Fluorescent calcium imaging methods have emerged as a powerful non-invasive tool for studying the synaptic network at cellular resolution. Somatic calcium influx generates action potentials within neurons that provide a way to detect and visualize neurophysiological and/or synaptic connectivity. Calcium imaging connectivity methods address certain drawbacks of multi-electrode recordings from electrophysiological (MEA *in vitro*; EEG, MEG *in vivo*) and functional magnetic resonance imaging techniques (fMRI *in vivo*) [7–18]. Specifically, high-impedance micro-electrodes can only capture the action potentials generated by closely proximal neurons with particular source-sink geometries; lower impedance electrodes can capture the activity of more distant neurons, albeit as a volume average from which the activity of more distant units cannot be definitively discriminated [10]. Calcium recordings permit simultaneous observation of numerous neurons at cellular resolution and can quantify the calcium activity of any neuron visualized, enabling more comprehensive study of neuronal networks through the monitoring of simultaneous interactions between active neuronal populations [10, 19, 20]. While functional calcium imaging does not address all shortcomings of MEA-based recordings, it has generally been shown to present a useful reflection of action potentials. For instance, whereas calcium imaging fundamentally reflects calcium ion flux and calcium ion propagation, in certain cases it can be used to infer action potential activity, as seen in studies by Lutcke *et al* [21] where spikes were reconstructed from calcium signals acquired even at low sampling rates of 20–30 Hz [21,

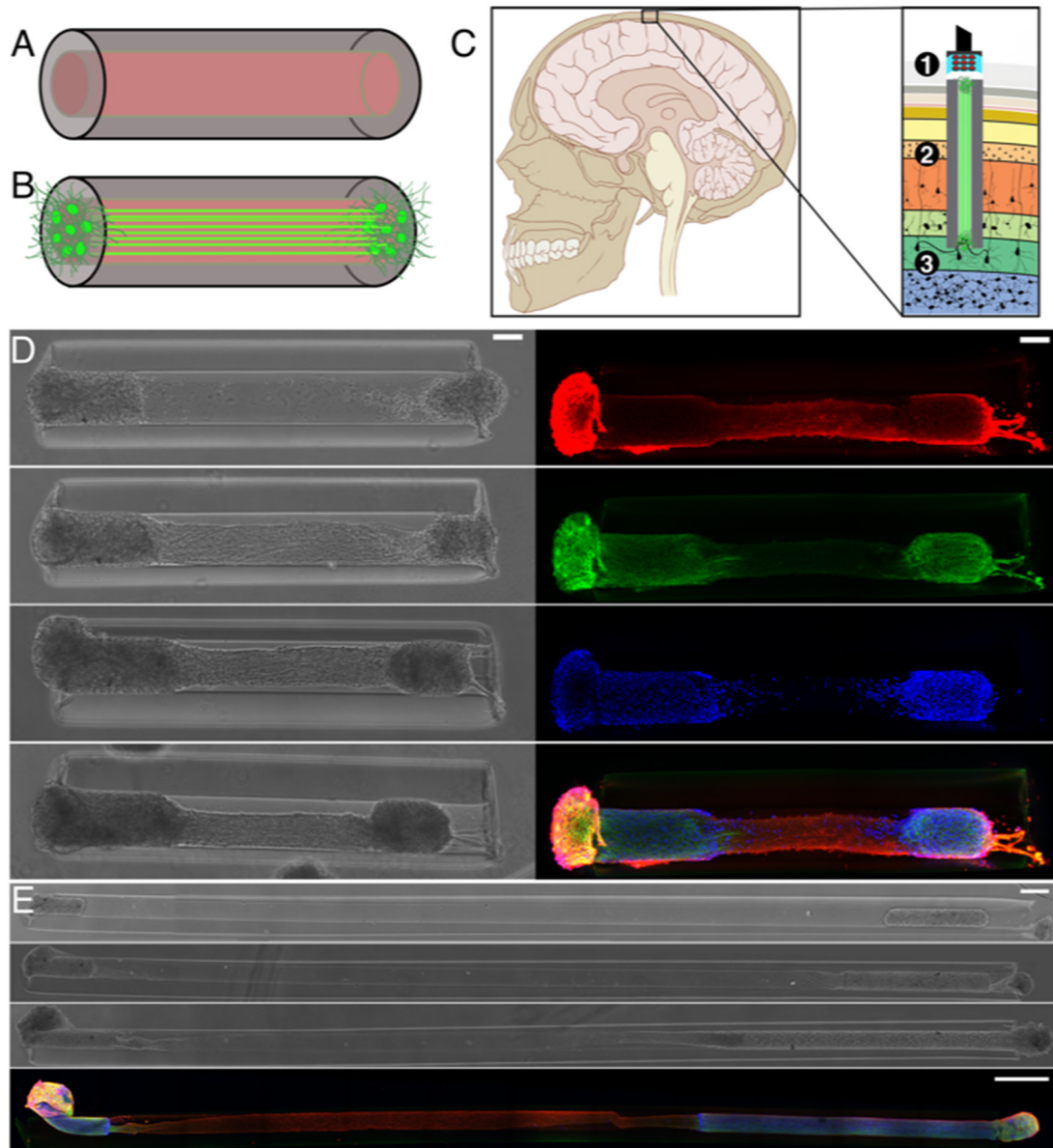


Figure 1. Micro-TENNs as a platform technology for brain pathway reconstruction or as ‘Living Electrodes’ [1, 4–6]. (A) Micro-TENNs initially consist of a 3D hydrogel cylinder (gray) encasing an extracellular matrix core of collagen and laminin (red), to date measuring up to several centimeters in length. (B) Bidirectional micro-TENNs have neuronal aggregates placed at both ends of the cylinder, with axonal tracts growing to span the cylinder length. (C) In the ‘Living Electrode’ paradigm, an optical probe may record activity (1) from vertically implanted bidirectional micro-TENNs (2) upon their synaptic integration with host neurons from specific cortical layers within the brain (e.g. Layer V) (3) (D) Left: phase microscopy images of a 1.5 mm bidirectional micro-TENN at 1, 3, 4, and 7 d *in vitro* (DIV). Right: confocal reconstructions of the same micro-TENN stained to identify axons (Tuj-1; red), cell soma/dendrites (MAP-2; green), and cell nuclei (Hoechst; blue). Scale bars: 100 μm . (E) Phase microscopy images of a ~9 mm bidirectional micro-TENN at 1, 3, and 7 DIV. The bottom image is a confocal reconstruction of this micro-TENN with the same labeling as in (D). Scale bars: 500 μm .

22]. Further advancements in the development of GECI’s (such as GCaMP6, used in the current study) have considerably improved the response kinetics, dynamic range and signal to noise ratio [23].

In the current study we have employed the use of calcium imaging signals and high-speed fluorescent microscopy to estimate connectivity patterns within micro-TENNs featuring discrete neuronal populations spanned by long-projecting, 3D axonal tracts. Methods to estimate functional connectivity included action potential recordings [24], cross-correlation, phase synchronization [25], coherence, transfer entropy (TE)

and Granger causality [26]. Many of these methods have previously been applied to investigate connectivity patterns in neural networks. For instance, Falli *et al* [27] conducted functional analysis on calcium imaging from a zebrafish spinal cord using cross-correlations and Granger causality methods. Similarly, Astolfi *et al* [12] demonstrated the use of the direct transfer function (DTF) method to estimate connectivity from EEG data signals. In the study by Dombbeck *et al* [20], correlation analysis was implemented on fluorescent calcium signals from awake, mobile mice, revealing strong cross-correlations among observed neuron signals and treadmill running activity.

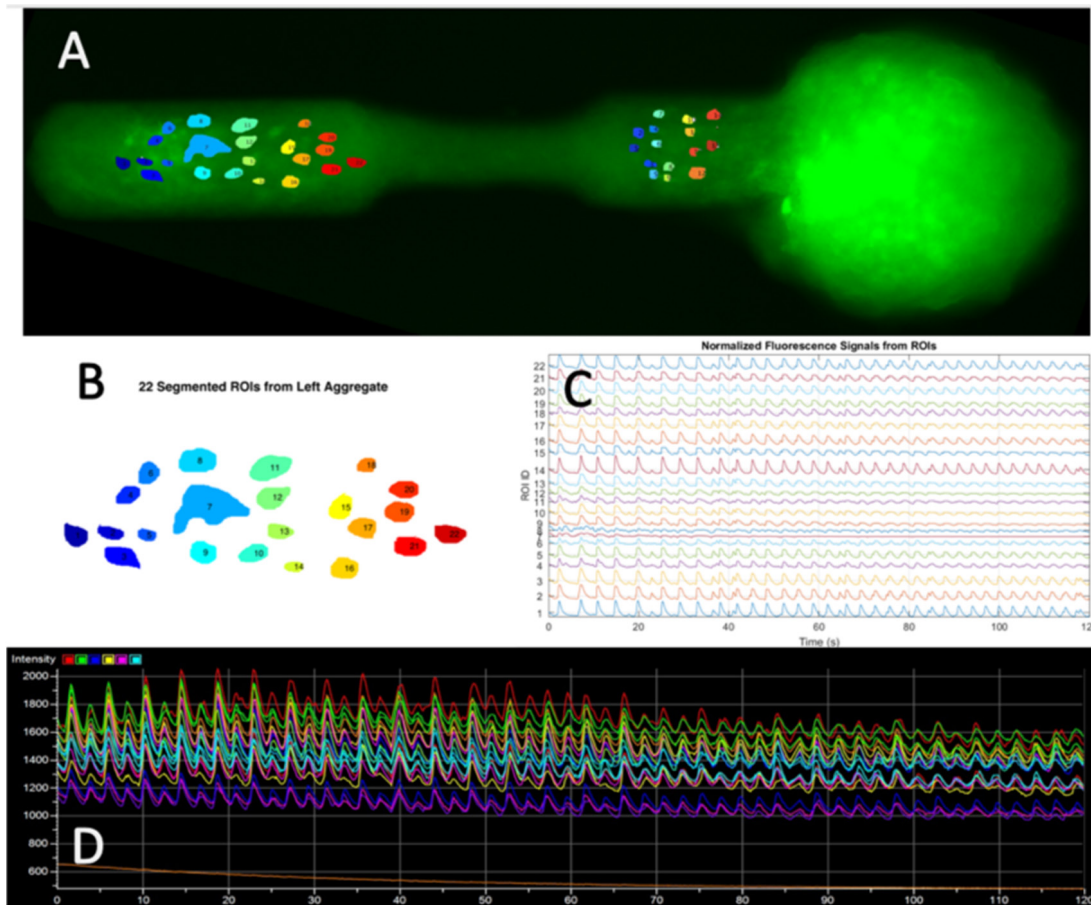


Figure 2. Micro-TENN ROI Image Segmentation. (A) Tiff stacks containing images of fluorescent calcium activity over time within micro-TENNs were imported into FluoroSNNAP. (B) Using image segmentation, ROIs within the aggregates were manually segmented. (C) FluoroSNNAP's automated spike detection methodology yielded normalized fluorescence ($\Delta F/F$) trace activity for the duration of the recordings. (D) Experimental calcium transients from the recordings were identified in NIS Elements. The intensities of selected ROIs were plotted over time relative to non-active background.

However, to our knowledge no previous studies have focused on estimation of functional connectivity using the DTF and TE methods applied to fluorescent calcium imaging of neuronal networks. Here, our objective is to establish a framework to quickly and efficiently analyze non-linear multivariate micro-TENN datasets to reveal activity levels and connectivity patterns in the future. This framework involves TE and DTF in conjunction with two additional functional connectivity methods: cross-correlation and phase synchronization. We assert that none of these methods are independently conclusive; rather, by implementing a combination of these techniques we can reliably estimate functional connectivity. Moreover, the non-directed and directed analyses complement each other and provide additional insights into information flow patterns. Additionally, electrophysiological processes exhibited by neural systems have similar oscillatory signal structures, making them well suited for frequency domain analysis [28]. Accordingly, in the current study we first describe the methods employed for estimating the functional connectivity within micro-TENNs. We provide detailed descriptions of the mathematical approach for applying these methods. Then, we describe results of applying the characterization techniques, discuss their implications, and note important limitations of our approach.

2. Materials and methods

2.1. Micro-TENN fabrication, staining, and image acquisition

Embryonic day 18 (E18) rat cortical neurons were extracted from brain tissue, dissociated, and forced into cell aggregates via centrifugation as previously described [6]. Aggregates were transduced with the genetically encoded calcium reporters GCaMP6f or RCaMP1b (Penn Vector Core, Philadelphia, PA). At 24 h post-transduction, aggregates were seeded within 3% agarose micro-columns (outer and inner diameters: 345 and 180 μm , respectively; length: 2–10 mm) that had been filled with a collagen-laminin extracellular matrix (1 mg ml⁻¹ each). In this study, aggregates were placed at both ends of each micro-column to create so-called 'bi-directional' micro-TENNs with two axonally-linked neuronal populations that were as long as the agarose micro-columns in which they were grown: 1.5 mm ($n = 7$) or 9–10 mm ($n = 3$) in length (figure 1). Micro-TENNs were then allowed to grow in neuronal culture media and monitored via phase and fluorescent microscopy to assess growth and calcium reporter expression. After 10 d *in vitro*, spontaneously active micro-TENNs were imaged on a Nikon Eclipse Ti confocal microscope paired with an ANDOR Neo/Zyla Camera through Nikon Elements AR

4.50.00 (Nikon Instruments). Micro-TENNs were recorded at ≥ 20 Hz for 120 s, with the resultant recordings exported as TIFF image stacks for data processing and analysis.

For immunocytochemistry, selected micro-TENNs were fixed in 4% formaldehyde in $1 \times$ PBS for 35 min. Post-fixation, micro-TENNs were rinsed with $1 \times$ PBS and permeabilized in 0.3% Triton X100 + 4% normal horse serum in $1 \times$ PBS for 1 h. Micro-TENNs were then incubated overnight at 4 °C with the primary antibodies beta-III tubulin/Tuj-1 (T8578, 1:500 dilution, Sigma-Aldrich) and microtubule-associated protein 2/MAP2 (AB5622, 1:500, Millipore). Micro-TENNs were subsequently rinsed in $1 \times$ PBS and incubated for 2 h at 18 °C–24 °C with fluorescently labeled secondary antibodies (1:500, Life Technologies). Micro-TENNs were then incubated with Hoechst (33342, 1:10000, ThermoFisher) for 10 min before being rinsed in $1 \times$ PBS and imaged on a Nikon A1RSI scanning confocal microscope paired with NIS Elements 4.50.00 (Nikon Instruments). All confocal images presented are maximum intensity projections of sequential slices along the z -axis; slices were 10–20 μm thick. Of note, the use of optical calcium recording has been shown to be a reliable approach to measure neuronal network activity as compared to electrical microstimulation [29].

2.2. FluoroSNNAP data processing

The acquired TIFF image stacks contained time-lapse images of fluorescent calcium activity collected for 120 s generating 2400 frames at 20 Hz sampling rate. We used FluoroSNNAP [30] open source software to perform image segmentation and spike detection to generate calcium signals from the regions of interest (ROIs). This was done by importing the TIFF stack into the software and manually defining the ROIs. Multiple bright-field ROIs were selected from a time-averaged image with an approximate size of 20 μm (figures 2(A) and (B)). Note that figures 2(B)–(D) are for the left side of the micro-TENN shown—similar plots exist for the right-hand side as well. In the next step, FluoroSNNAP computed normalized fluorescence trace waveforms representing calcium transient activity (figure 2(C)). The software delineates neuronal activity from a baseline fluctuation and produces waveforms using a database of known transient waveforms. This discriminates calcium activities from other intercellular sources. Since active neurons were selected based on the standard deviation of the fluorescence signal for the length of the recording, the number of considered regions could differ across distinct micro-TENNs (figure 2(A)). ROI shapes were selected by two or more investigators based upon visual inspection of luminance fluctuation following the methodology from [30].

2.3. Methods for estimating functional connectivity

Briefly, there are three main types of connectivity studies used to describe the inter communication between brain regions or neuronal populations: structural, functional and effective connectivity. Friston [15] puts forward definitions between functional and effective connectivity to outline

distinct differences between the two measures. Functional connectivity is defined as the temporal correlation of measured signals from spatially remote neurophysiological events. Functionally connected neural networks exhibit synchronized activity patterns measured using various linear and non-linear computational tools such as cross-correlation, coherence, Granger causality and transfer entropy (TE). These methods are useful in measuring the existence and summarizing the types of interactions that are recorded from activity within the neuronal population [14, 31].

Effective connectivity is a specific form of functional connectivity. It is defined as the simplest independent model of system component interactions used to generate temporal relationships as observed experimentally. Effective connectivity is used to postulate the consequences of coupling actions. In the case of micro-TENNs, effective connectivity measures would allow us to postulate and model the network structure. However, in order to verify the accuracy of model, neuron stimulation and high-resolution imaging techniques are required. Therefore, based on the experimental limitations of maintaining live neuron cultures during the stimulation process, we focused our study on fundamental functional connectivity analysis to quantify the temporal relationship between different loci of calcium influx activity within the micro-TENN.

2.3.1. Pearson cross-correlation. Pearson cross-correlation is the most common non-directed time-domain linear measure of interaction (a detailed description of the mathematics of this approach is included in the supplementary material). The computation of higher correlations implies greater functional relationships between the related neuronal populations. This method does not always identify causal relationships but is a computationally robust and inexpensive tool to determine network synchronizations [32, 33].

2.3.2. Phase Synchronization. To infer the synchrony among the neuron populations, we computed phase synchronization to estimate dependencies between n ROI signals. This method was based on calculating the instantaneous phases through Hilbert transformation of signals [34] and applying the synchronization equation derived by Allefeld [35]. That is, the phase synchronization R_{ij} of two oscillators i and j can be defined as the peak of the distribution of the phase difference $\phi_{jl} - \phi_{il}$:

$$R_{ij} = \left| \frac{1}{n} \sum_{l=1}^n \exp(i(\phi_{jl} - \phi_{il})) \right| \quad (1)$$

where $l = 1 \dots n$ enumerates the realizations in given sample and takes values from 0 to 1. In our study, the two oscillators i and j represents the two ROI signals selected. Pearson cross-correlation and phase synchronization are used to infer non-directed synchronous patterns in the micro-TENN ROIs. Phase synchronization has previously been demonstrated both *in vitro* and *in vivo*, including from cortical and hippocampal

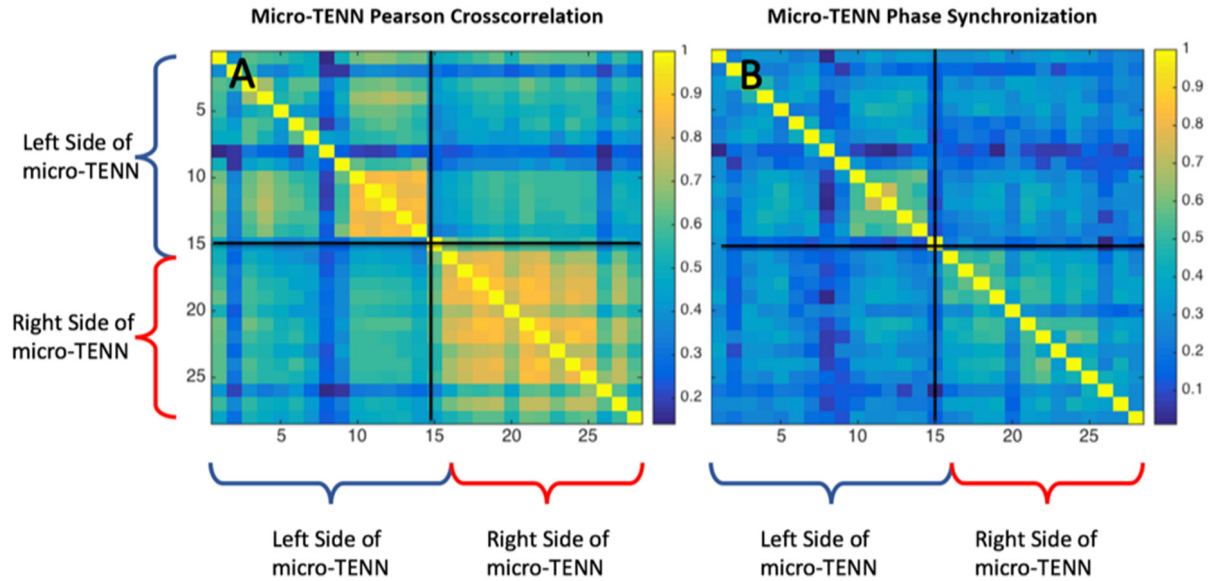


Figure 3. Micro-TENN pearson cross-correlation (A) and phase synchronization (B). The plots are divided into four sub-blocks. ROIs 1...15 are from one aggregate of the micro-TENN (i.e. left cluster of ROIs in figure 2(A)) and 16...30 from the other aggregate (i.e. right cluster of ROIs in figure 2(A)). The diagonal elements represent Pearson cross-correlation and phase synchronization within the region itself, while the off-diagonal blocks represent the different regions. The Pearson cross-correlation matrix reveals high correlation values (greater than 0.5). Note that Pearson cross-correlation goes from -1 (anti-correlation) to $+1$ (perfect correlation), with 0 indicating no correlation. In this case, we observe high correlation between micro-TENN ends that produce no values below zero. Similarly, the phase synchronization plot reveals high synchronicity values (greater than 0.8) between the ROIs' signals.

local field potentials, and whole cell voltage clamp recordings of thalamic neurons [36, 37].

2.3.3. Directed transfer function (DTF) and power spectral analysis. Kaminski and Blinowska [38] first introduced Directed Transfer Function formulations to estimate the direction of information flow activity (appendix A). The normalized DTF (nDTF) method can be used to estimate directed information flow within the neural network [9, 16, 39, 40]. Directed Transfer Function is defined as the causal influence of channel j on channel i at frequency f . The normalized version of DTF, nDTF, takes values from 0 to 1 producing a ratio between the inflow from channel j to channel i to all the inflows to channel i . Therefore, using the DTF approach, we can provide evidence for direction of activity flow between micro-TENN structures as a function of frequency. In this method, a spectral transfer matrix is computed from a fitted multichannel autoregressive (MVAR) model [10]. The SIFT-EGLAB manual [41] presents several information criterions for the user to estimate an appropriate model order to fit the data. Briefly, these include akaike information criterion (AIC), schwarz bayes criterion (SBC), final prediction error criterion (FPE), and hannan-quinn criterion (HQ). In other words, we interpret information flow from the estimated MVAR coefficients fitted on the original calcium signal data. One of the major advantages of nDTF analysis is the unrestricted limitation to analyze many channels in different frequency bands. Since our dataset involves a considerable number of ROI calcium signals, this feature proves to be useful. Power Spectrum reveals the network's connectivity strength as a function of frequency based on the original signal data [42–45]. Power spectrum analysis of the calcium signals was calculated using

fast Fourier transformation (appendix B). Power Spectrum analysis results were used to verify the relevancy of nDTF MVAR model results.

2.3.4. Transfer entropy (TE). To verify the results obtained by the previous methods, we also employed transfer entropy (TE) method [46–48] to quantify information transfer within the cortical aggregates of the micro-TENN. Recent work on TE developed by Kaiser and Schreiber [46] highlights the mathematical formulations and advantages of TE on continuous signal processes namely when TE method takes into account the linear and non-linear information flows to define causality strength between two signals. Orlandi et al [48] demonstrates the use of TE method to study functional connectivity interactions for simulated calcium imaging signals. Similarly, Gourevitch et al [47] employed TE methodology to study information transfer between auditory cortical neurons. They analyzed spike trains from 16 recording sites from the auditory cortex of 21 ketamine-anesthetized cats with recording signal length of 900s. Transfer entropy metrics have also revealed patterns of information flow between thalamus and cortex in the anesthetized rat [49]. In our case, we use this tool to investigate spontaneous non-stimulated activity of up to 30 ROI signals collected from the micro-TENN. Transfer Entropy results were obtained using the Java Information Dynamics Toolkit (JIDT) toolbox [50].

3. Results

To focus on synchronizing properties between these signals, Pearson cross-correlation (figure 3(A)) and phase synchronization studies (figure 3(B)) were computed. All data analyses

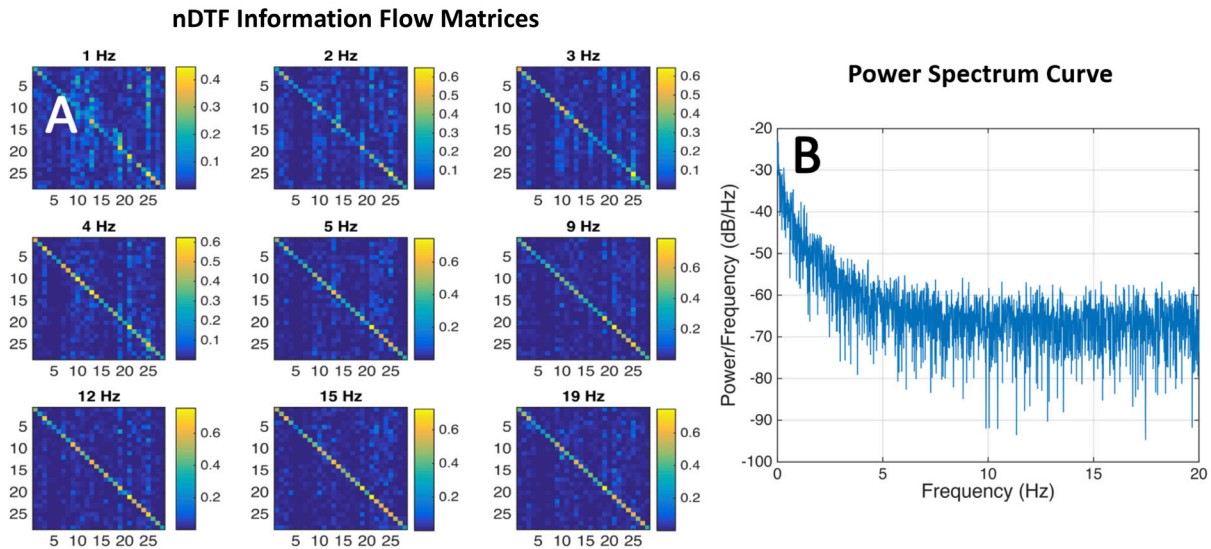


Figure 4. Micro-TENN nDTF (A) and power spectral analysis (B). The nDTF information flow matrix: the diagonal elements represent information flow within the region itself while the off-diagonal block represents the cross-talk information flow across the micro-TENNs. The nDTF matrices at frequencies 19 Hz: at each frequency, both diagonal and off-diagonal blocks are non-empty indicating information flow within the left and right regions and across the micro-TENN. This is more prominent at frequencies between 1 to 4 Hz (delta frequency). (B) Power spectral frequency analysis reveals stronger signal power frequencies 1–5 Hz in correspondence with DTF analysis.

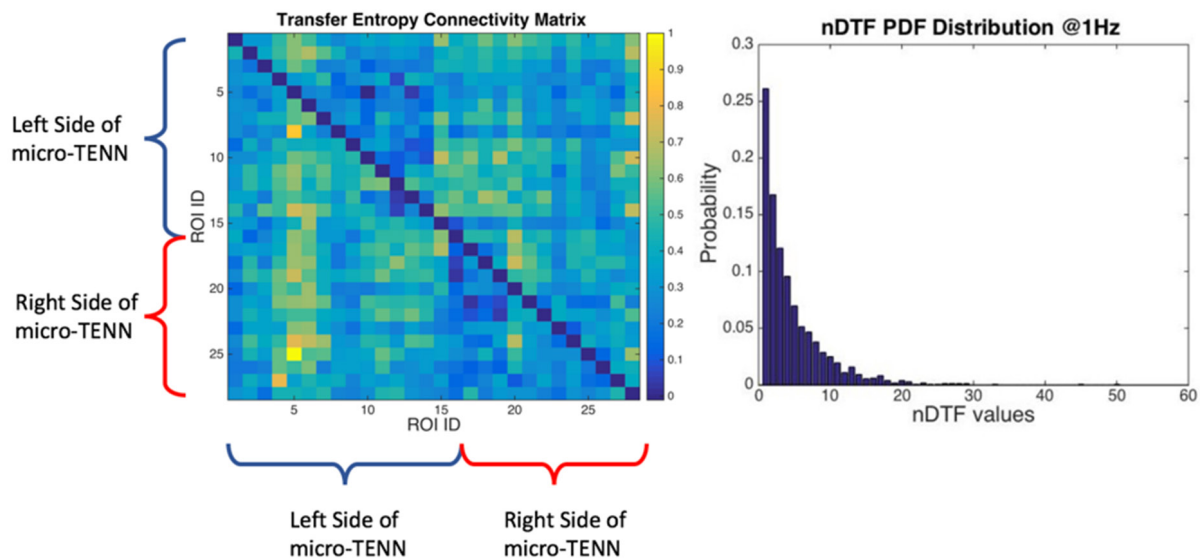


Figure 5. (A) Micro-TENN transfer entropy and (B) probability density distribution. Transfer Entropy connectivity metrics suggest dynamical dependence between the calcium signals. These results are visually consistent with the phase synchronization plot. Probability density distribution from the information flow nDTF matrices obtained using different micro-TENN images were collected at varying frequencies and growth days. Positively skewed distribution shows excitatory-only connectivity patterns within the micro-TENN.

include intra- and cross-population measurements for every pair of ROIs. The computation of higher correlations implies greater functional relationships between the related neuronal populations. Both studies generated values of cross-correlation and phase synchronization greater than 0.8, suggesting that micro-TENN aggregates exhibit synchronous activity and have a high probability of being functionally connected.

To further infer causal dependencies between the calcium firing patterns within the micro-TENN neuronal aggregates ROIs, normalized directed transfer function (nDTF) connectivity matrices were generated using the EEGLAB SIFT

[42] multivariate autoregressive (MVAR) model fitted to the signals. The nDTF method can be used to estimate directed information flow within the neural network [9, 16, 39, 40]. In our case, we use it to estimate the information flow across the micro-TENN construct. The nDTF estimates were obtained by using a numerically stable 10th order MVAR model with an 80 s sliding window length and 40 s time step (appendix A). The nDTF coefficients were obtained over the frequency band between 1 to 9 Hz. Given these parameters, nDTF matrices revealed information flow across the micro-TENN particularly for frequencies 2 to 5 Hz (figure 4(A)). Time varying

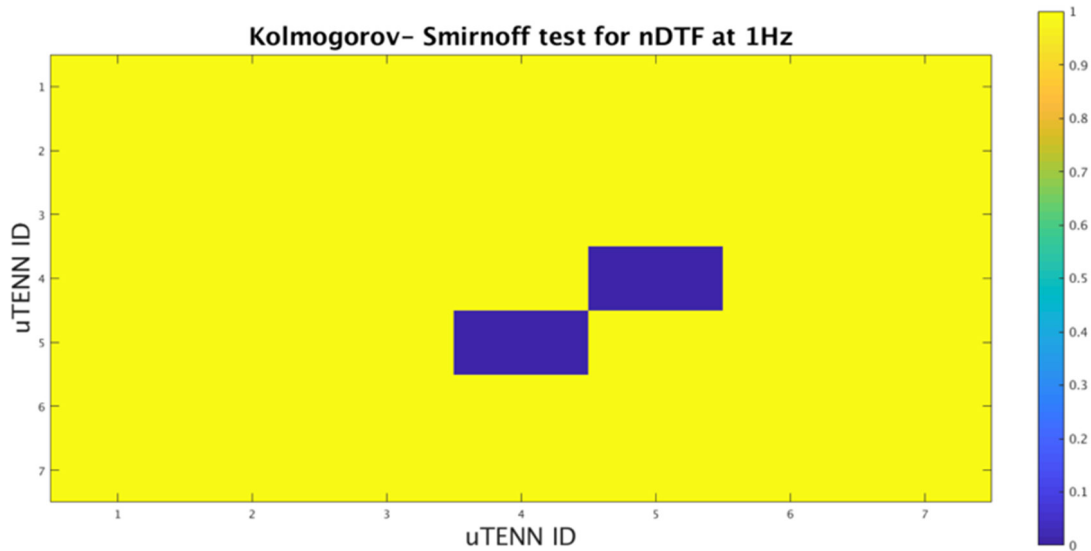


Figure 6. Results of pairwise Kolmogorov–Smirnov test (KST) on the nDTF values at 1 Hz for a p -value of 0.01 for all the micro-TENNS.

power spectrum analysis revealed the strength of information propagation at various frequencies. Signal power strength is visible at elevated peak levels for dominant delta (1–4 Hz) and theta (4–8 Hz) frequency bands and progressively weakens at higher frequencies (figure 4(B)). These signal power strength results closely matched nDTF analysis where near synchronous information flow was detected between frequencies 2 to 5 Hz.

Observing neural oscillations at distinct low frequencies has broad impact on cognitive multiplexing processes [51] such as memory performance [52] and regulating large-scale networks [53]. In the case of micro-TENNS, information flow across different frequencies suggest mechanisms of neural multiplexing communication whereby multiple information streams share a common neural substrate. Similar results have been found in *in vitro* models of the brain connectome, wherein paired clusters of cortical neurons formed complex intercellular circuits and exhibited multiplexed input responses [54].

Multivariate model independent TE calculation was based on continuous-valued micro-TENN data using the kernel-estimator [51]. Transfer entropy is an additional metric that may reveal patterns of information flow between ROIs. The TE connectivity matrix (figure 5(A)) revealed distinct sub-blocks representing the two micro-TENN aggregates and non-zero mutual information transfer across the aggregates. Results computed using DTF and TE in the functional connectivity framework have delivered consistent results (figure 5(B)) demonstrating that neuronal aggregates within micro-TENN have dynamic coupling connectivity.

This same series of analysis tools was carried out on six additional micro-TENNS (individual results included in appendix C). For all seven micro-TENNS, we performed a pairwise Kolmogorov–Smirnov test (KST) on the nDTF values at 1 Hz (a dominant activity frequency in the micro-TENNS) as shown in figure 6. The KST is a nonparametric test comparing the probability distributions of the samples for a

given statistical significance level, in this case $p = 0.01$. Since the KST does not require any preliminary knowledge about the probability distributions of the samples, it is suitable for comparison of the activity patterns across the different micro-TENNS. We applied the KST to test the hypothesis that the given micro-TENN nDTF datasets are from the same distribution (a value of 1 indicates that two samples have similar probability distributions of nDTF, whereas a value 0 indicates that the probability distributions are not similar). This analysis showed that of all the possible comparisons across the different micro-TENNS, all yielded a value of 1 (showing consistent nDTF probability distributions) with the exception of a single comparison (micro-TENN 4 versus micro-TENN 5). This suggests that the patterns of activity or communication are similar across all of the micro-TENNS at this time point and frequency, with the exception of a single pair where the nDTF patterns were statistically different (although these ‘different’ micro-TENNS were similar to the others). In these different functioning micro-TENNS, the activity patterns could become more similar as the neuronal networks continue to mature and/or similar activity patterns could be occurring at different frequencies.

4. Discussion

Micro-TENNS are anatomically-inspired constructs designed to structurally and functionally emulate white matter pathways in the brain. As such, they are being developed to be transplanted *en masse* to reconstruct and/or modulate damaged axonal pathways as well as to serve as biofidelic test-beds to study neurophysiology and/or pharmacologic interventions in an anatomically-relevant, yet controlled *in vitro* setting. This paper provides the first report of functional connectivity of distinct neuronal populations via long-projecting, 3D axonal tracts based on fluorescent calcium activity analyzed via novel application of nDTF and TE methods. These functional data

are a crucial step to not only understanding tactics employed for information flow across 3D axonal tracts, but also for the future development of ‘all-optical’ techniques for probing and modulating these networks based on the addition of optogenetic techniques for controlled stimulation. Collectively, this improved understanding and precisely engineered control will allow us to further improve the design and optimization of implantable neural networks that could ultimately be deployed to reconstruct the nervous system to treat neurological disease and injury.

Synchronous neuronal activity appears critical for certain behaviorally relevant computations, while hypersynchrony can impair information coding and cause epileptiform responses [36]. Synchronization of neural populations has been shown not to require a common driving source and instead relies on the length of the tract connecting them, the number of cells involved, and upon the mixture of recurrent and feedforward connections [37, 55]. The cross-correlation and phase synchronization analysis of calcium signaling in the micro-TENN suggests a strong degree of synchronous co-activation within a cluster, and to a lesser yet still significant degree, synchronous co-activation between the two clusters as mediated by the axon tracts (figures 3(A) and (B)). The apparent difference in synchronization between and within the two neural populations of the micro-TENNs (i.e. the two clusters of ROIs seen in figure 2(A)) also implies that the spatial geometry afforded by the micro-TENN fabrication induces a kind of functional segregation while simultaneously sustaining functional connectivity. This pattern is in contrast to dissociated cultures which tend to form hypersynchronized bursting networks [56]. The micro-TENN mixture of synchronization results mirror results seen previously in dissociated neuron cultures grown on MEAs that have physical barriers to promote regional clustering [57] and of organotypic slice cultures [58], with the crucial distinction that micro-TENNs are 3D, self-contained constructs that can be implanted into the brain as a unit [3].

The nDTF and TE analyses demonstrated that information (entropy) flows within and between the cluster populations of the living micro-TENN and this flow has an asymmetric directionality (anisotropy) (figures 4 and 5). These results reveal that the micro-TENN spontaneously exhibits information flow dynamics across the long, 3D axonal tracts that is analogous to what has previously been described *in vivo* [47, 49]. In addition to these results being inherently interesting as a first characterization of a novel bioengineered axon-based construct, they also provide a crucial baseline necessary before proceeding to analyzing micro-TENN activity once implanted and allowed to integrate *in vivo*. Indeed, the *in vitro* results hence form a kind of ‘null hypothesis’ ‘deafferented’ state that can inform interpretation of calcium imaging and other physiological assays once deployed *in vivo* either to anatomically reconstruct missing/damaged brain pathways or as a ‘living electrode’ for biological/synaptic-based modulation of deep neural circuitry.

In order to demonstrate the robustness of the analysis tools presented in this paper, we analyzed functional connectivity

by applying the same suite of analyses in six additional individual micro-TENNs (included in appendix C). Based on these additional analyses, our major findings and conclusions do not change for 5 of the 6 additional micro-TENNs. That is, we see cross- and phase-synchronization, information flow as shown by nDTF and cross-communication (or cross-talk) as shown by transfer entropy. However, the 6th additional micro-TENN that we examined was particularly interesting: we observed high correlation, synchronization and communication within the ends of the micro-TENN, however, we observe limited cross-talk between the ends of this micro-TENN (referred to as micro-TENN 07 in appendix C). We noticed in this case that the right side of micro-TENN 07 had two distinct regions with significant activity in each and that they were not synchronized (observed visually). It appeared as there were two functional systems at one end of the micro-TENN—a kind of smaller micro-TENN system within a larger micro-TENN system. So, anatomically this micro-TENN was somewhat different than the others, nonetheless, the reasons for limited cross-talk across the ends for this micro-TENN are unknown. There could be competition occurring between functional regions, with the two sub-regions on the right side being initially more coupled since they were closer together. It is also possible that long-distance cross-talk may develop with different timing in this system and therefore would manifest at a later time post-planting, which will be the scope of future work. In total, these additional findings support that primary conclusions of the paper and demonstrate generalized axon-based interconnectivity across the discrete neuronal populations in bidirectional micro-TENNs.

Of note, the functional connectivity analysis described here could be applied to other tissue engineered constructs and in fact provides an approach/framework to compare the functional physiology of a variety of engineered constructs with each other and with *in vivo* recordings, in a manner that complements static imaging and histology. In this particular case of the micro-TENNs, our analysis approach confirms the presence of a repertoire of connectivity patterns more complex than found in dissociated cultures and suggests that intentionally designed 3D scaffolds—mimicking features of gray matter to white matter architecture—can induce connectivity patterns with more *in vivo*-like features.

5. Limitations

In this paper, we demonstrate a framework for understanding the synaptic connectivity of micro-TENNs via information flow across long, integrated, 3D axonal tracts. We established a process using correlation, phase synchronization, power spectrum, TE and DTF methods to study calcium fluorescent signals efficiently. By implementing DTF method, we were able to establish that the majority of the micro-TENN information transfer between aggregates occurs at frequency levels 1–5 Hz. However, it is plausible that a number of limitations may arise from two main factors: temporal-spatial resolution and firing rate. First, the experimental resolution of the high-speed

images captured by our confocal microscope system was limited by trade-offs between acquisition rate and resolution, as well as optical/diffraction limitations of the visible spectrum. Inevitably, this limits our ability to structurally identify cell membranes where calcium action primarily occurs. Aggressive imaging techniques can potentially cause permanent photobleaching that can damage or kill the live tissue. Another limitation arises from the inherent slow time constant decay of calcium indicators, restricting the ability to capture high frequency activity as noticed in the power spectral analysis. Despite these limitations, converging results obtained from a combination of all the functional methods applied to study the micro-TENNs suggest there is compelling evidence of functional information transfer within and across the aggregates. This functional methods framework will support our future work to quickly process large sample sizes, assess functional categorization at various stages of micro-TENN development/growth, and assess connectivity patterns across numerous micro-TENNs linked together to replicate complex 3D circuits in the brain. Importantly, this will allow us to establish a functional baseline immediately prior to implantation into the brain while not directly contacting the constructs, which could compromise their structural integrity and/or sterility. Of note, our findings agree with Poli *et al* [59], who also applied correlation methods and TE to establish network connectivity and concluded that no single method was inferior or superior in assessing the neuronal network properties, but it was useful to apply these in combination while interpreting the findings based on limits of applicability of the chosen methods.

Another limitation is that the current paper only validates these methods for a single 3D neural construct design. However, we should note there are many alternative approaches for creating 3D engineered nervous tissue. Excellent reviews are given by Zhuang *et al* [60], Hopkins *et al* [61] and Schmidt and Leach [62]. A few popular technologies that are being investigated include spheroids [63–65], organoids [66–68], and scaffold-based constructs for which there are extensive types of materials studies, ranging from gelatin [69] to silk [70, 71]. In addition, microfluidic [72] and bioprinting-based constructs [73] are also being investigated. It would be interesting to explore the methods presented herein for evaluating functional connectivity for these complimentary approaches to 3D neural tissue fabrication.

6. Conclusions

We presented a novel approach to characterize micro-TENN connectivity using multiple methodologies such as transfer entropy (TE) and directed transfer function (DTF) analysis on calcium imaging signals. To date, most of the functional connectivity techniques presented in this paper have been previously established for *in vivo* neuroimaging analysis, here we demonstrate and validate their applicability to analyze calcium activity across 3D axonal tracts spanning

discrete neuronal networks. This analysis framework demonstrated that micro-TENNs exhibit cross-talk activity using multiple information transfer metrics. These results suggest functional connectivity across engineered 3D axonal tracts, and significantly contribute to the overall functional characterization of cortical neuronal networks in micro-TENNs to support their application to reconstruct white matter pathways or as anatomically-fidelic test-beds of long-distance brain networks.

Acknowledgments

Financial support was provided by the National Institutes of Health through the Brain Initiative [U01-NS094340 (Cullen and Kraft)], the National Science Foundation through a Graduate Research Fellowship [DGE-1321851 (Adewole)], and the US Department of Defense through the Congressionally Directed Medical Research Program [JPC8-CRMRP #W81XWH-16-1-0796 (Cullen)]. Computations for this research were performed on the Pennsylvania State University's Institute for CyberScience Advanced CyberInfrastructure (ICS-ACI).

Author contributions

DKC, MDS and RHK conceived the project, designed the experiments, and provided general supervision. DOA generated micro-TENNs and performed all transfection, staining, and imaging experiments. AVD, AHWC, TM designed and performed data analysis routines. AVD, MDS, DOA, RHK, and DKC contributed to drafting and editing the manuscript.

Conflicts of interest

The authors declare no conflict of interest. The funding sponsors had no role in the design of the study; in the collection, analyses, or interpretation of data; in the writing of the manuscript; or in the decision to publish the results.

Supplementary materials

The code for this study can be found at: <https://github.com/PSUCompBio/microTENN-FC>.

Appendix A

A.1. Normalized directed transfer function (nDTF) method

The DTF technique is applied to a set of cortical estimated waveforms dataset S obtained for N ROIs considered [12, 16].

$$S = [s_1(t), s_2(t), \dots, s_N(t)]^T. \quad (\text{A.1})$$

Table C1. Summary of findings for all micro-TENNs.

Micro-TENN ID	Pearson cross-correlation (PCC)	Phase synchronization (PC)	Normalized directed transfer function (nDTF)	Transfer entropy (TE)
High/low definitions	Cross micro-TENN PCC values > 0.5 (%)	Cross micro-TENN PC values > 0.5 (%)	Off-diagonal values of nDTF at 1 Hz > 0.005 (%)	Off-diagonal TE values > 0.05 (%)
1 (discussed in main body of manuscript)	59	31	85	100
2	100	100	55	94
3	100	100	79	99
4	100	100	70	100
5	100	100	85	100
6	100	100	95	100
7	0	0	34	100

The following MVAR model is fitted on the estimate waveforms dataset S under the condition that $\mathbf{E}(t)$ is a vector of multivariate zero mean uncorrelated white noise process.

$$\sum_{k=0}^p \Lambda(k) S(t-k) = \mathbf{E}(t) \text{ with } \Lambda(0) = 1 \quad (\text{A.2})$$

where $\Lambda(1), \Lambda(2), \dots, \Lambda(p)$, are the $N \times N$ matrices of model coefficients where p is the model order chosen by information criterion. Next, the equation is transformed into the frequency domain to investigate the spectral properties of the examined process.

$$\Lambda(f) S(f) = \mathbf{E}(f) \quad (\text{A.3})$$

where

$$\Lambda(f) = \sum_{k=0}^p \Lambda(k) e^{-j2\pi f \Delta t k}. \quad (\text{A.4})$$

Therefore, equation (A.4) can be rewritten as:

$$S(f) = \Lambda^{-1}(f) \mathbf{E}(f) = \mathbf{H}(f) \mathbf{E}(f). \quad (\text{A.5})$$

$\mathbf{H}(f)$ is the transfer matrix of the system, whose element H_{ij} characterizes the connection between the j th input and the i th output of the system. With these definitions, the causal influence of cortical waveform estimated in j th ROI waveform on that estimated in i th ROI is defined as:

$$\theta_{ij}^2(f) = |H_{ij}(f)|^2. \quad (\text{A.6})$$

In order to compare the results obtained across different power spectra, these values are normalized from 0 to 1, where the normalization factor is defined by the sum along the rows of the spectral transfer matrix.

$$\gamma_{ij}(f) = \sqrt{\frac{|H_{ij}(f)|^2}{\sum_{m=1}^k |H_{im}(f)|^2}} \quad (\text{A.7})$$

where $|H_{ij}(f)|$ is an element of $\hat{H}(f)$ matrix ($H_{ij} \neq H_{ji}$). The squared sum of all elements of the relevant row in the denominator of equation (A.7) normalizes $\gamma_{ij}(f)$ in the range

from 0 to 1. γ_{ij} expresses the ratio of influence of the cortical waveform estimated in the j th ROI on the cortical waveform estimated on the i th ROI with respect to the influence of all waveforms.

Appendix B

B.1. Power spectrum method

The power spectrum $S_{xx,j}$ is defined as the magnitude squared of the Fourier transform of the data [16]. The power spectrum $S_{xx,j}$ is defined as the magnitude squared of the Fourier transform of the data [44].

$$S_{xx,j} = \frac{2\Delta^2}{T} X_j X_j^* \quad (\text{B.1})$$

where Δ is sampling interval, T is the duration of recording and X_j is the Fourier transform of x at frequency $f_i(X_i)$. The units of power spectrum here is $\mu\text{V}^2 \text{Hz}^{-1}$.

Frequency resolution and Nyquist Frequency are two important measures to consider when computing the power spectrum. The first term is the reciprocal of the total recording duration and latter is defined as half of the sampling frequency. The Nyquist frequency sets the limits for the highest observable frequency value one can detect in the analysis.

Appendix C

We analyzed functional connectivity in six additional individual micro-TENNs in order to demonstrate the robustness of the analysis tools presented in this paper. These findings support that primary conclusions of the paper and demonstrate generalized axon-based interconnectivity across the discrete neuronal populations in bidirectional micro-TENNs. Table C1 summarizes our results and the raw data can be found on the following pages. Figures C1–C12 provide raw and post-processed details on the additional micro-TENNs 2–7.

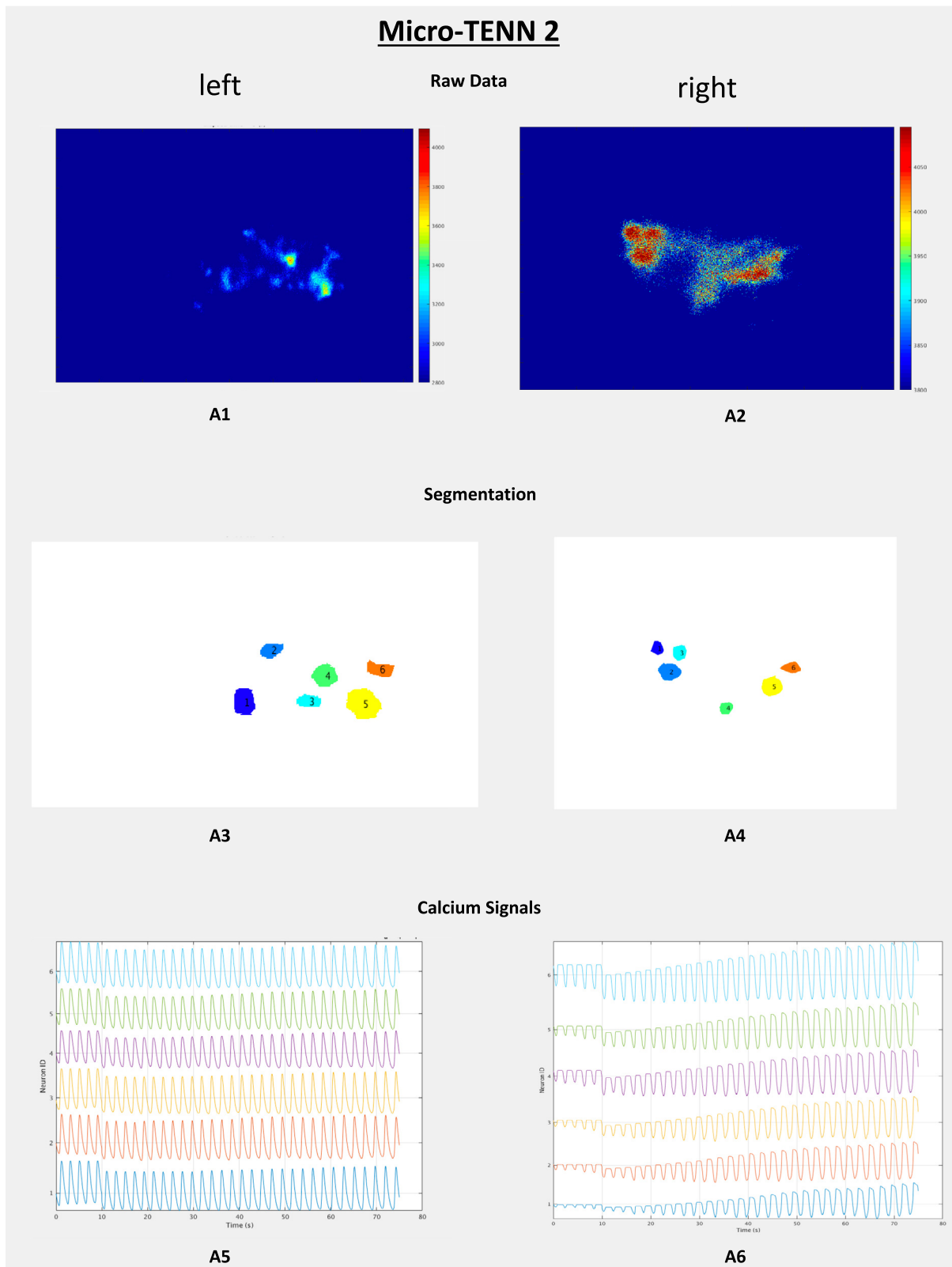


Figure C1. Micro-TENN 2 processing results. (A1) Left calcium imaging concentration contours visible in FluoroSNNAP and (A2) right calcium imaging. (A3) Left ROIs after segmentation and (A4) right ROIs after segmentation. (A5) Normalized fluorescence ($\Delta F/F$) trace activity for the duration of the recordings for left side of micro-TENN and (A6) normalized fluorescence ($\Delta F/F$) trace activity for the duration of the recordings for right side of micro-TENN.

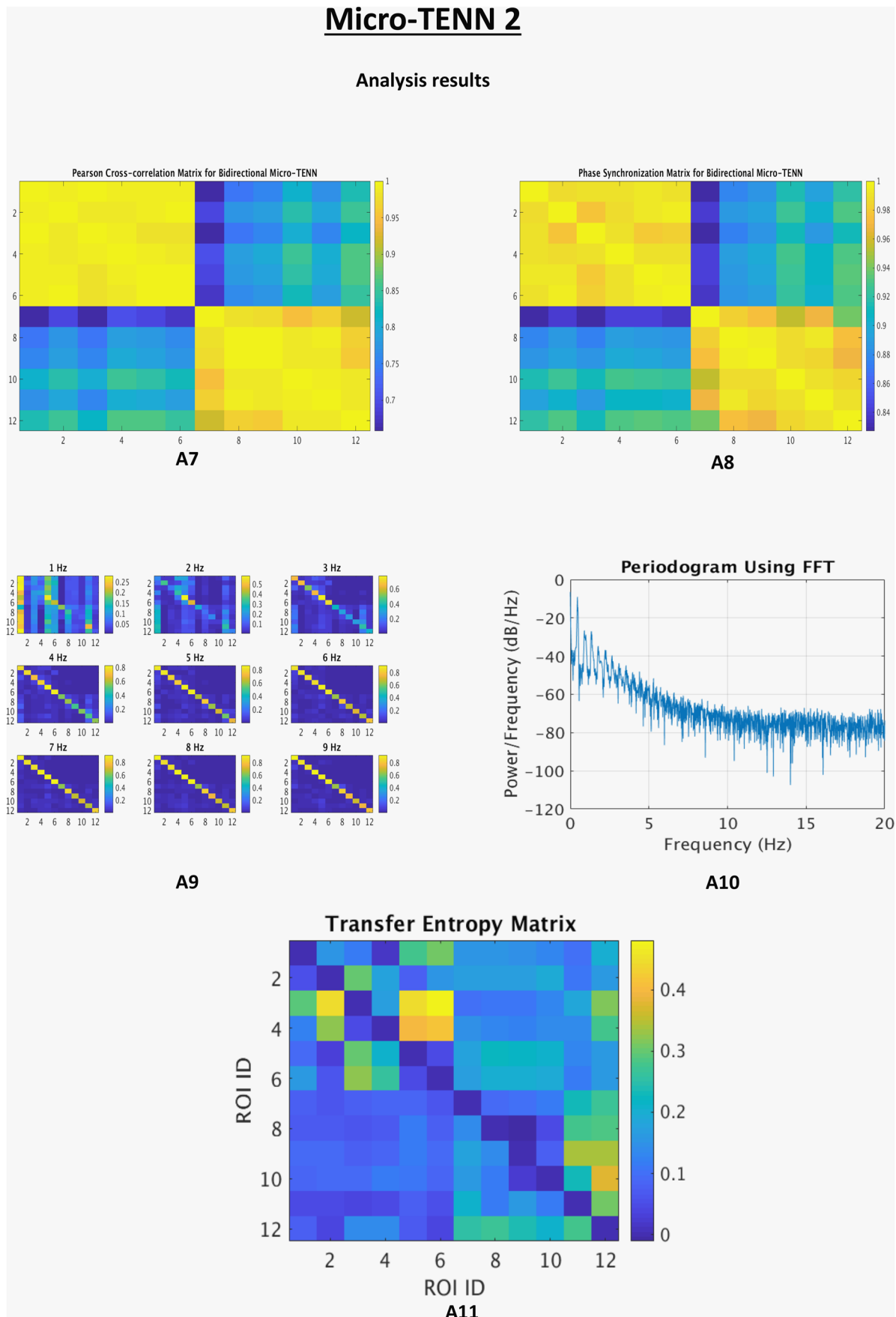


Figure C2. Micro-TENN 2 processing results, continued. (A7) Pearson cross-correlation and (A8) phase synchronization. (A9) Power spectral analysis and (A10) nDTF information flow matrix. (A11) Transfer entropy connectivity matrix.

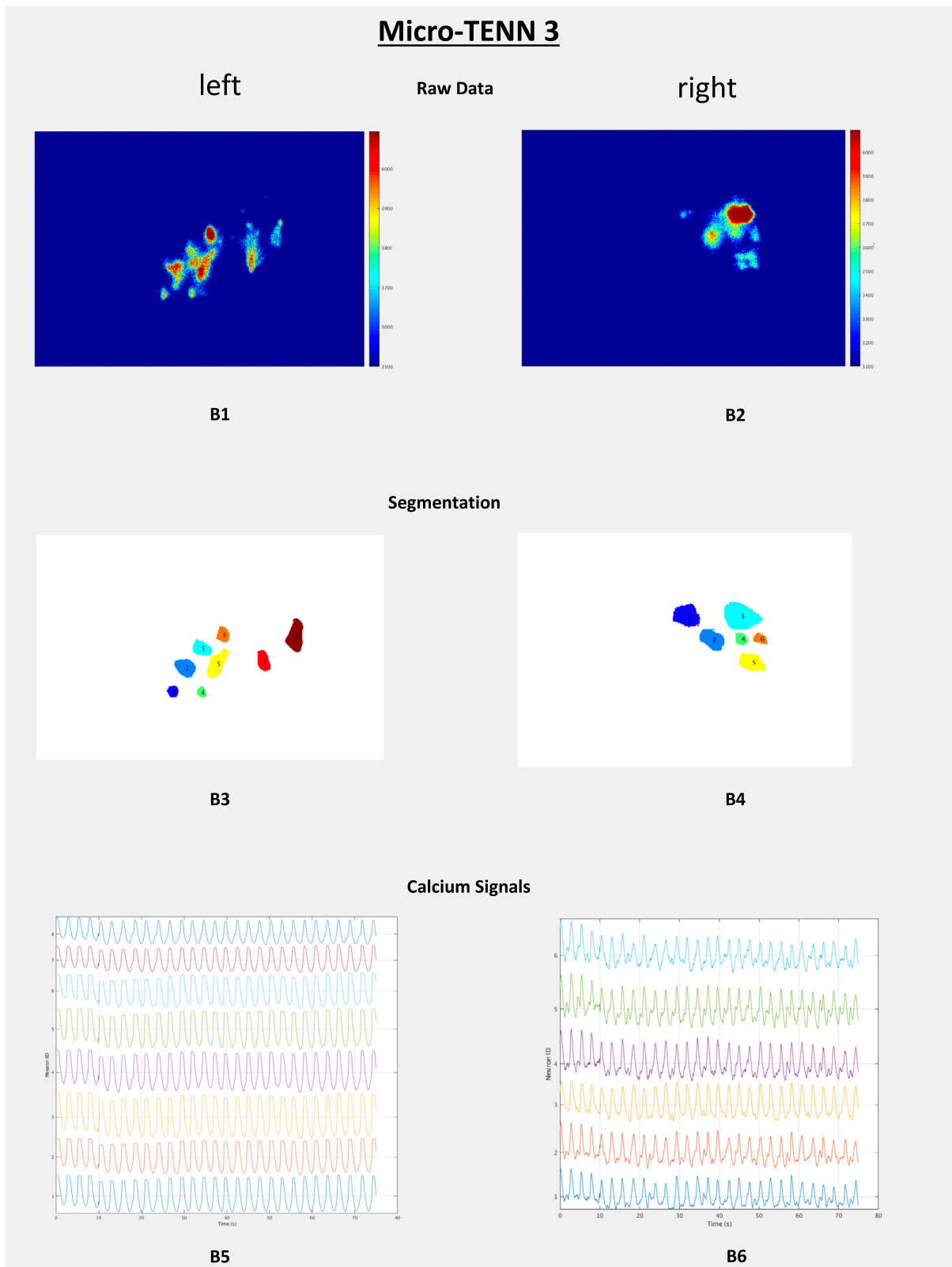


Figure C3. Micro-TENN 3 processing results. (B1) Left calcium imaging concentration contours visible in FluoroSNNAP and (B2) right calcium imaging. (B3) Left ROIs after segmentation and (B4) right ROIs after segmentation. (B5) Normalized fluorescence ($\Delta F/F$) trace activity for the duration of the recordings for left side of micro-TENN and (B6) normalized fluorescence ($\Delta F/F$) trace activity for the duration of the recordings for right side of micro-TENN.

Micro-TENN 3

Analysis results

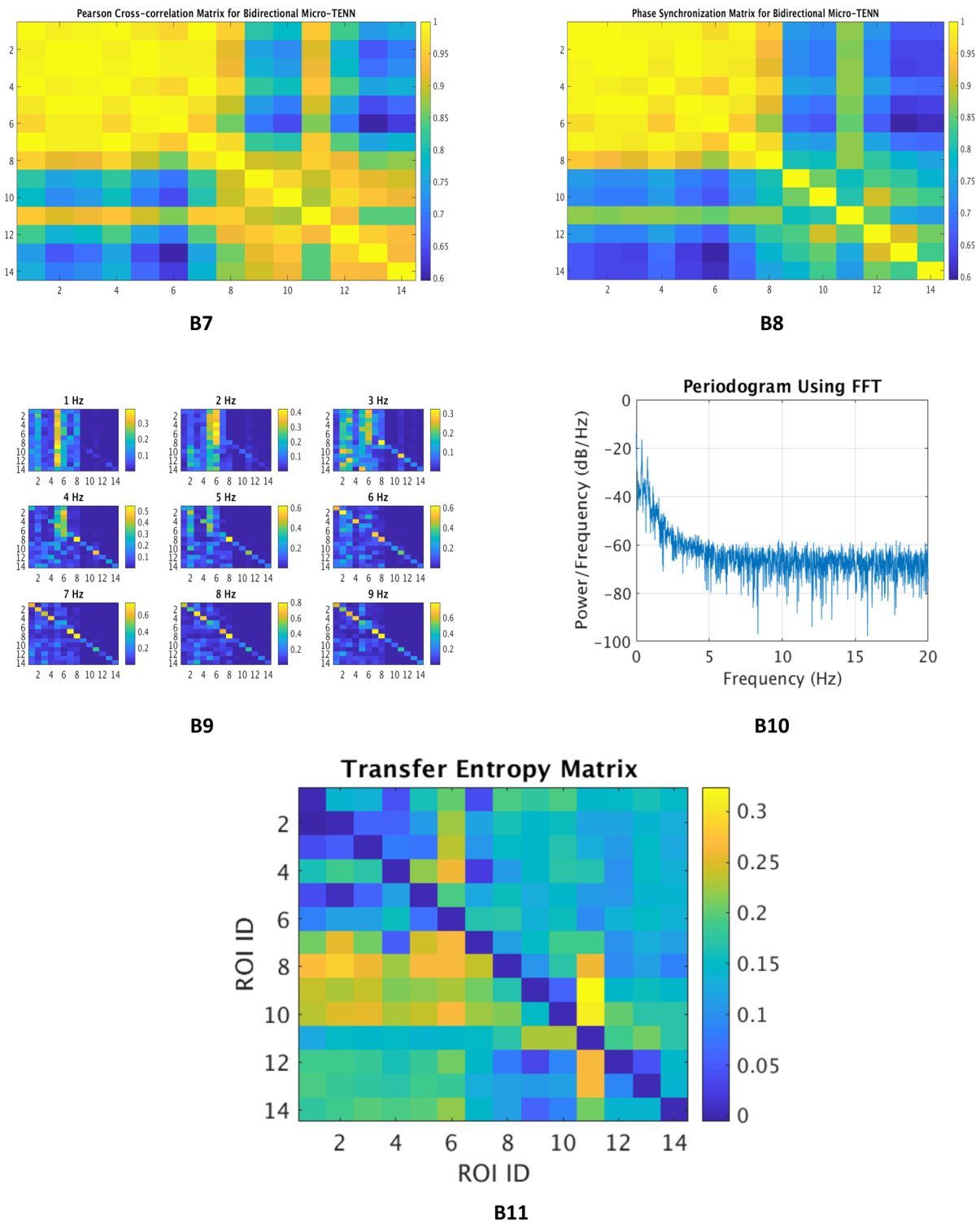


Figure C4. Micro-TENN 3 processing results, continued. (B7) Pearson cross-correlation and (B8) phase synchronization. (B9) Power spectral analysis and (B10) nDTF information flow matrix. (B11) Transfer entropy connectivity matrix.

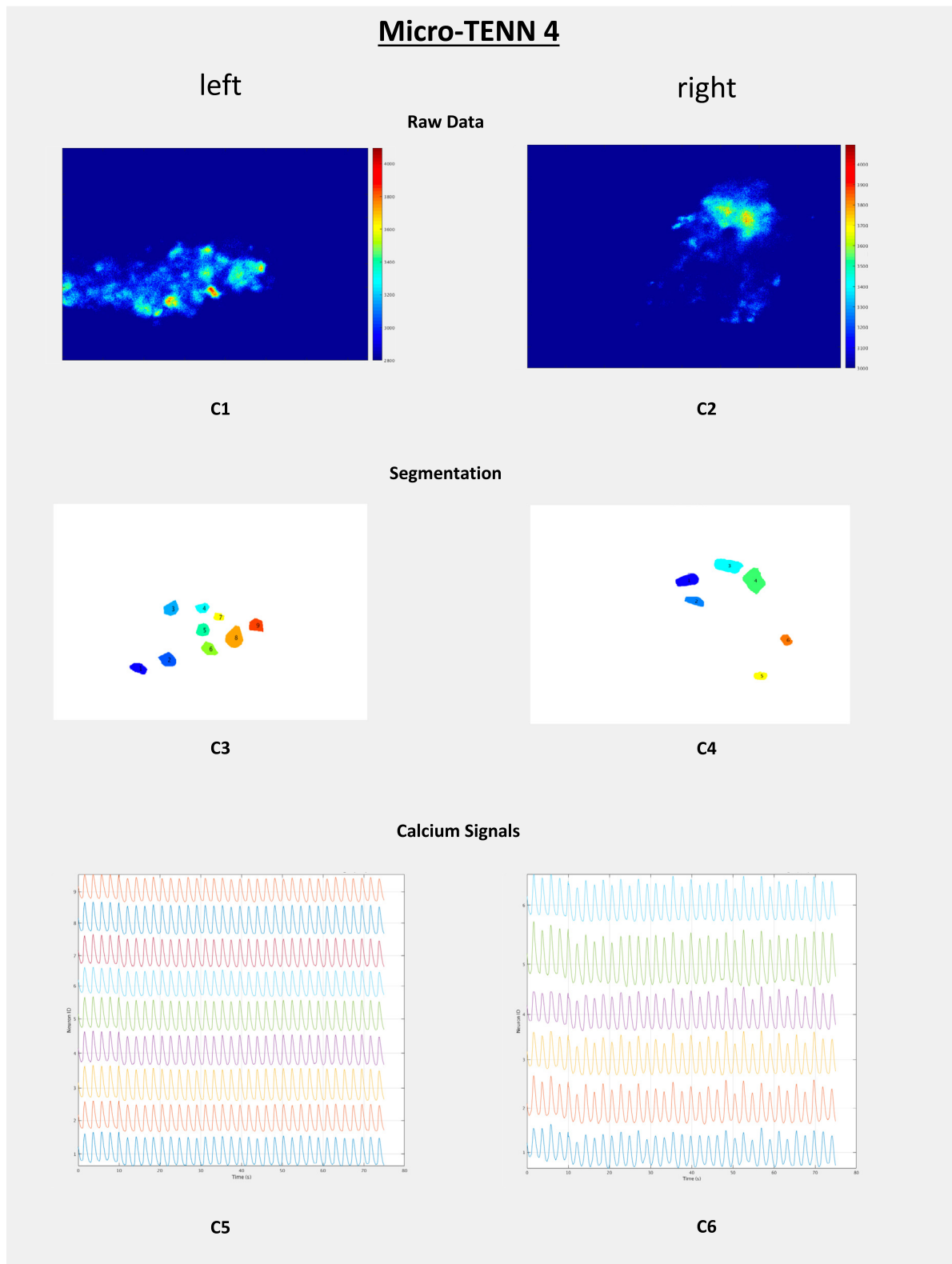


Figure C5. Micro-TENN 4 processing results. (C1) Left calcium imaging concentration contours visible in FluoroSNNAP and (C2) right calcium imaging. (C3) Left ROIs after segmentation and (C4) right ROIs after segmentation. (C5) Normalized fluorescence ($\Delta F/F$) trace activity for the duration of the recordings for left side of micro-TENN and (C6) normalized fluorescence ($\Delta F/F$) trace activity for the duration of the recordings for right side of micro-TENN.

Micro-TENN 4

Analysis results

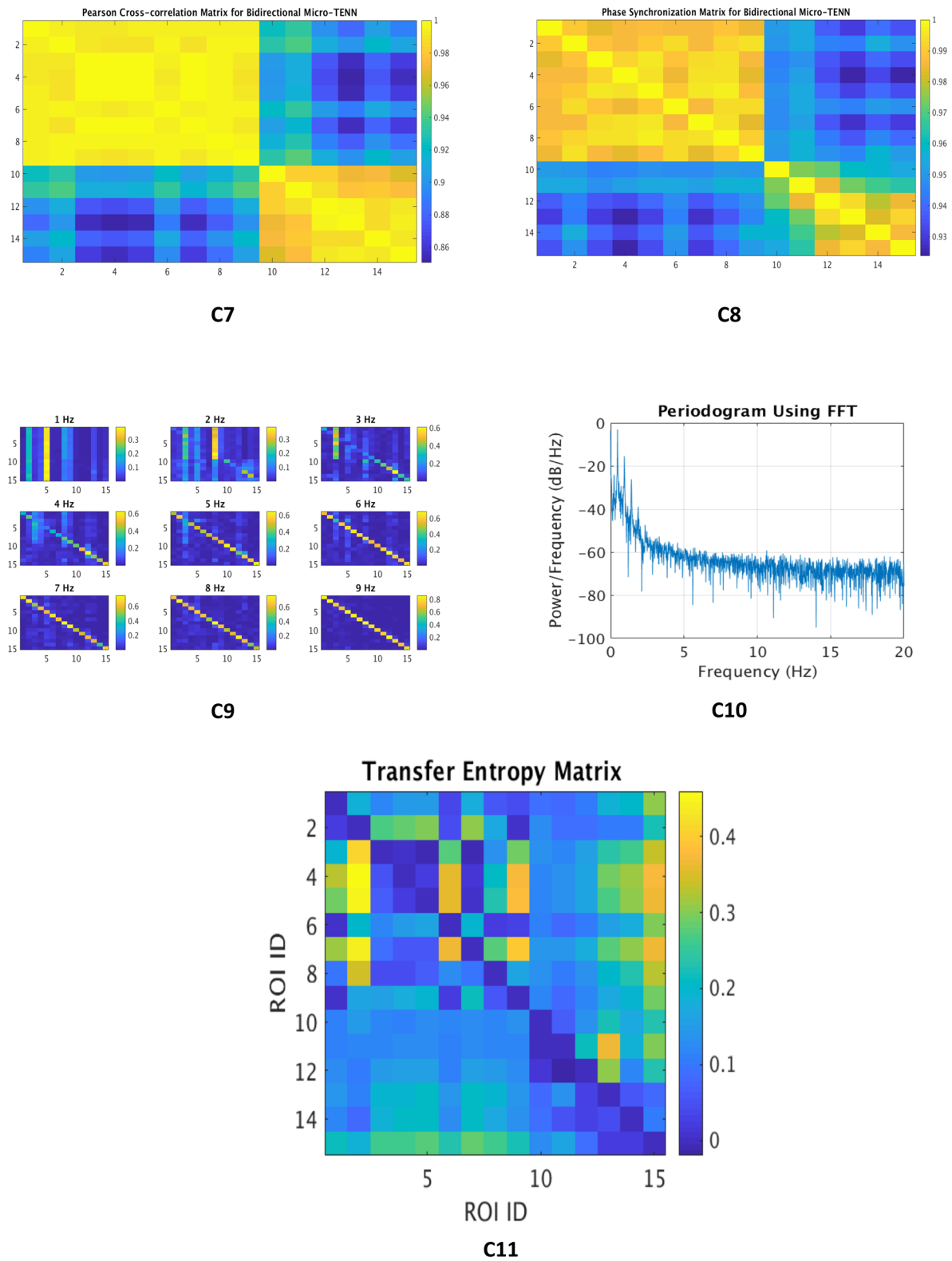


Figure C6. Micro-TENN 4 processing results, continued. (C7) Pearson cross-correlation and (C8) phase synchronization. (C9) Power spectral analysis and (C10) nDTF information flow matrix. (C11) Transfer entropy connectivity matrix.

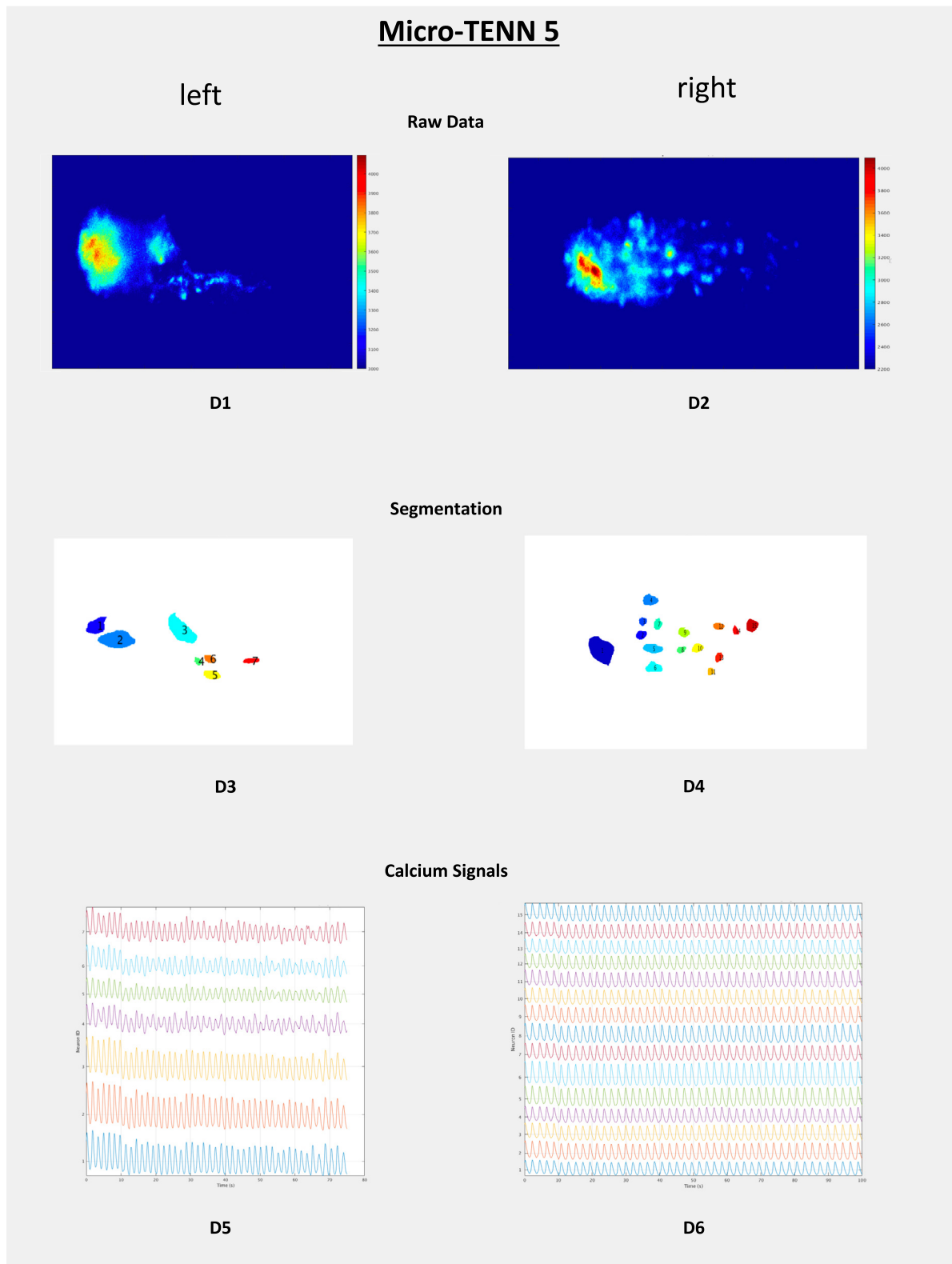


Figure C7. Micro-TENN 5 processing results. (D1) Left calcium imaging concentration contours visible in FluoroSNNAP and (D2) right calcium imaging. (D3) Left ROIs after segmentation and (D4) right ROIs after segmentation. (D5) Normalized fluorescence ($\Delta F/F$) trace activity for the duration of the recordings for left side of micro-TENN and (D6) normalized fluorescence ($\Delta F/F$) trace activity for the duration of the recordings for right side of micro-TENN.

Micro-TENN 5

Analysis results

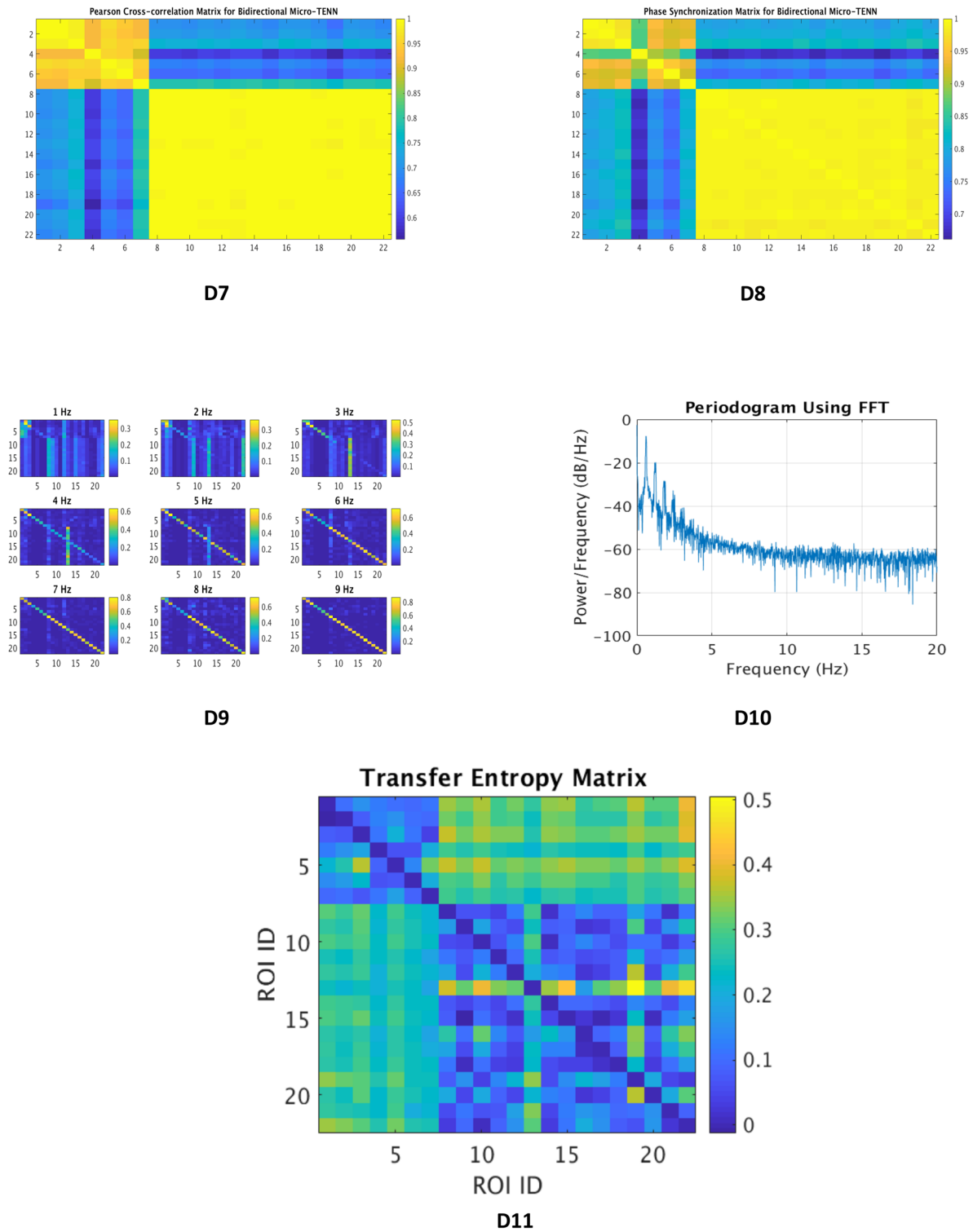


Figure C8. Micro-TENN 5 processing results, continued. (D7) Pearson cross-correlation and (D8) phase synchronization. (D9) Power spectral analysis and (D10) nDTF information flow matrix. (D11) Transfer entropy connectivity matrix.

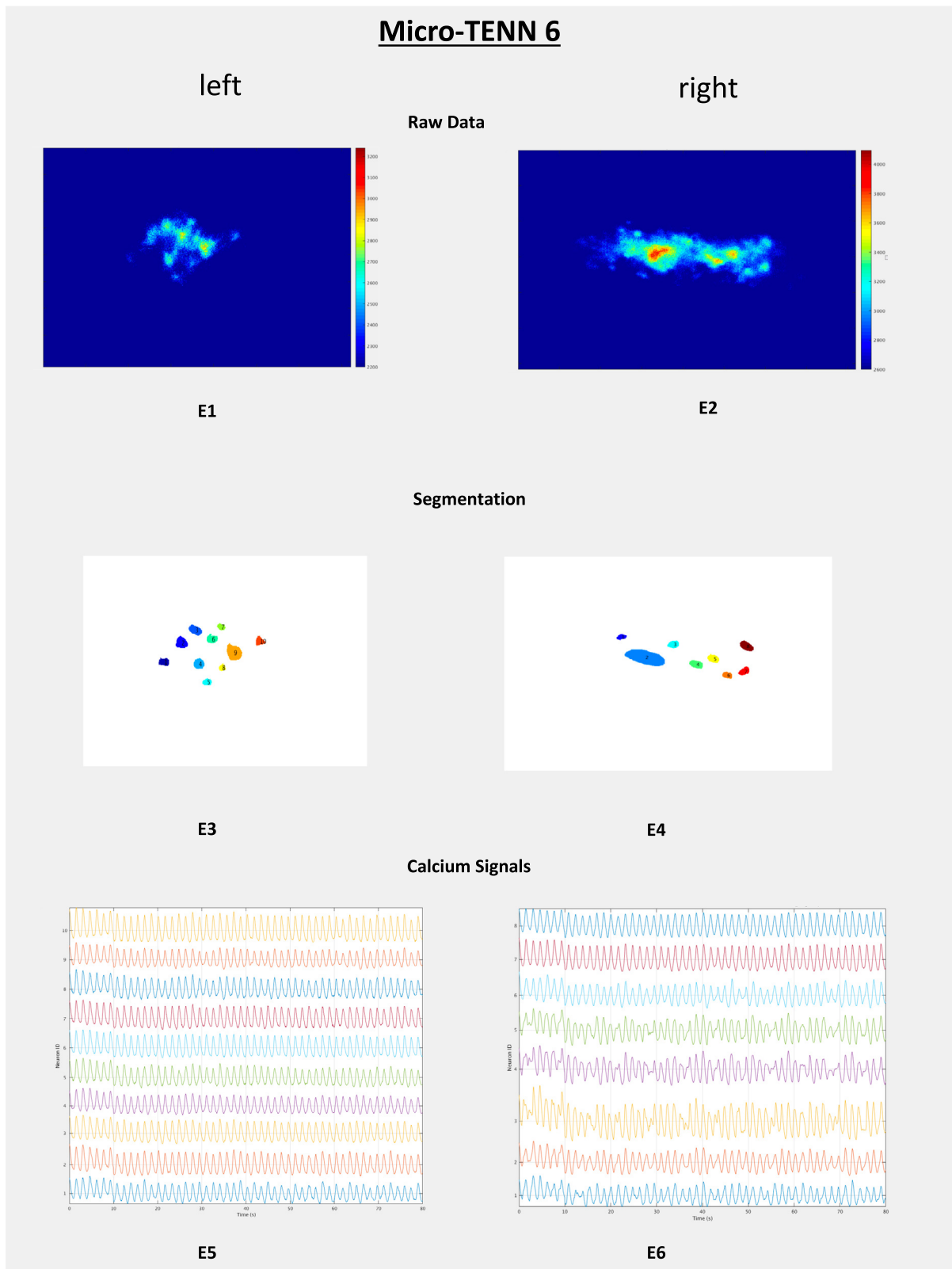
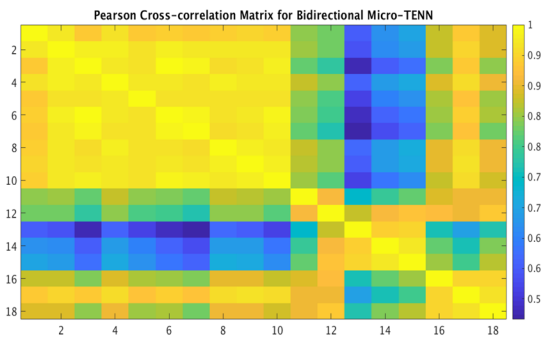


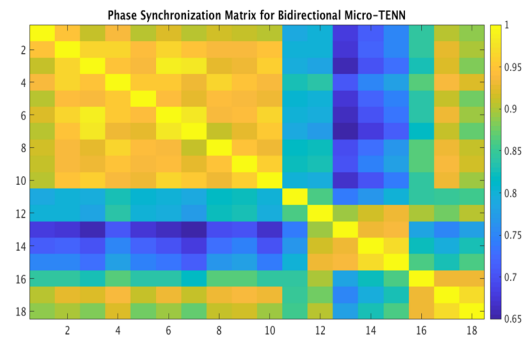
Figure C9. Micro-TENN 6 processing results. (E1) Left calcium imaging concentration contours visible in FluoroSNNAP and (E2) right calcium imaging. (E3) Left ROIs after segmentation and (E4) right ROIs after segmentation. (E5) Normalized fluorescence ($\Delta F/F$) trace activity for the duration of the recordings for left side of micro-TENN and (E6) normalized fluorescence ($\Delta F/F$) trace activity for the duration of the recordings for right side of micro-TENN.

Micro-TENN 6

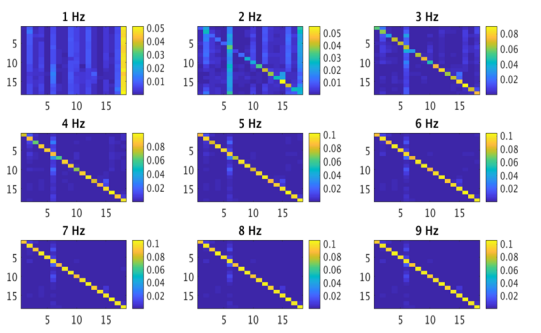
Analysis results



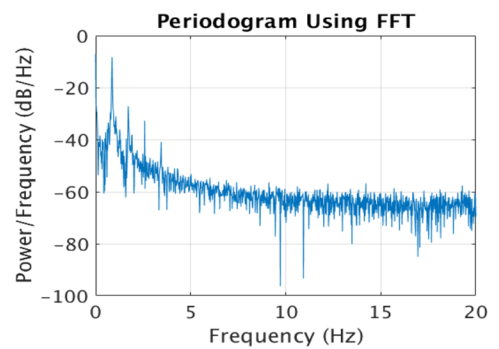
E7



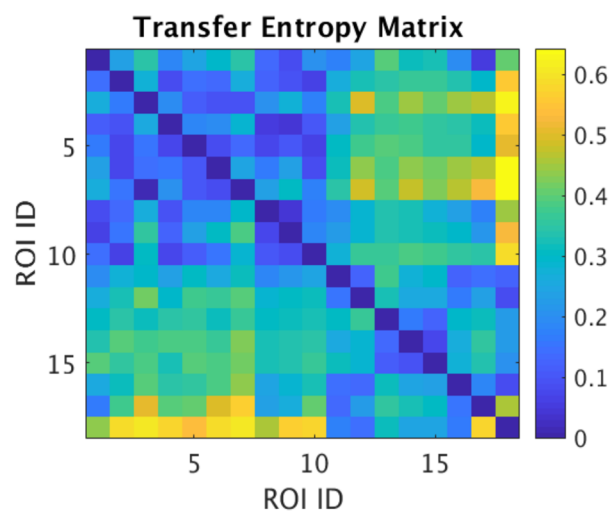
E8



E9



E10



E11

Figure C10. Micro-TENN 6 processing results, continued. (E7) Pearson cross-correlation and (E8) phase synchronization. (E9) Power spectral analysis and (E10) nDTF information flow matrix. (E11) Transfer entropy connectivity matrix.

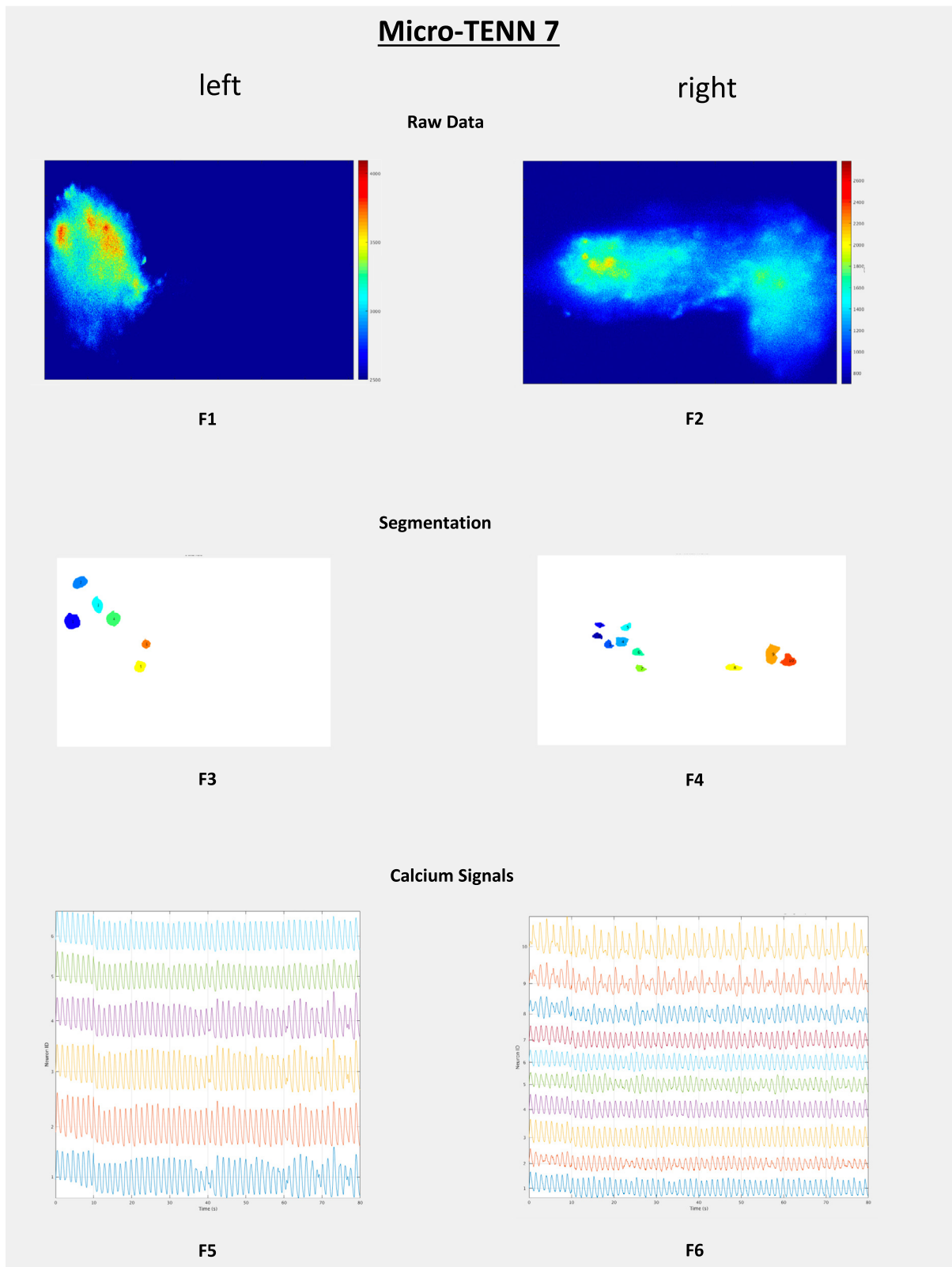
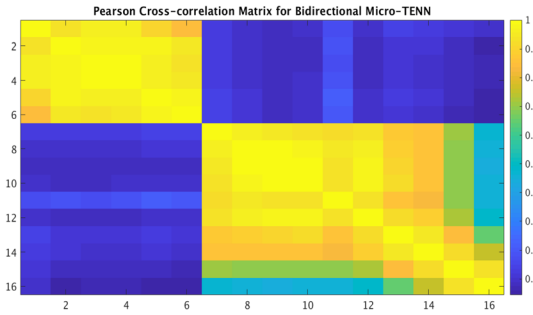


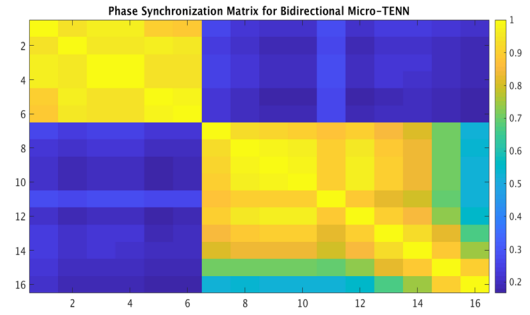
Figure C11. Micro-TENN 7 processing results. (F1) Left calcium imaging concentration contours visible in FluoroSNNAP and (F2) right calcium imaging. (F3) Left ROIs after segmentation and (F4) right ROIs after segmentation. (F5) Normalized fluorescence ($\Delta F/F$) trace activity for the duration of the recordings for left side of micro-TENN and (F6) normalized fluorescence ($\Delta F/F$) trace activity for the duration of the recordings for right side of micro-TENN.

Micro-TENN 7

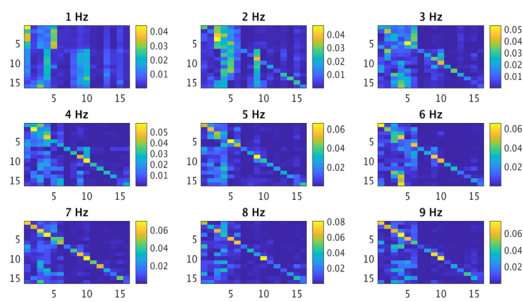
Analysis results



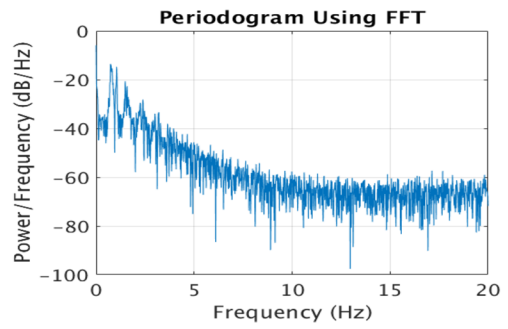
F7



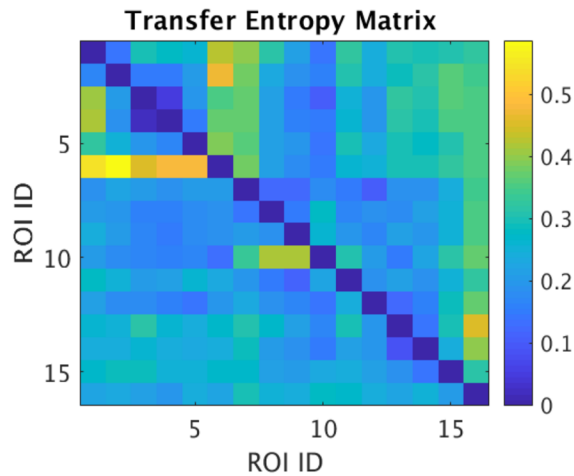
F8



F9



F10



F11

Figure C12. Micro-TENN 7 processing results, continued. (F7) Pearson cross-correlation and (F8) phase synchronization. (F9) Power spectral analysis and (F10) nDTF information flow matrix. (F11) Transfer entropy connectivity matrix.

ORCID iDs

Reuben H Kraft  <https://orcid.org/0000-0001-8211-0681>

References

- [1] Struzyna L *et al* 2015 Rebuilding brain circuitry with living micro-tissue engineered neural networks *Tissue Eng.* **21** 2744–56
- [2] Harris J P, Struzyna L A, Murphy P L, Adewole D O, Kuo E and Cullen D K 2016 Advanced biomaterial strategies to transplant preformed micro-tissue engineered neural networks into the brain *J. Neural Eng.* **13** 016019
- [3] Cullen D K *et al* 2012 Microtissue engineered constructs with living axons for targeted nervous system reconstruction *Tissue Eng. A* **18** 120817094501006
- [4] Serruya M D *et al* 2017 Engineered axonal tracts as ‘Living Electrodes’ for synaptic-based modulation of neural circuitry *Adv. Funct. Mater.* **28** 1701183
- [5] Adewole D O *et al* 2016 The evolution of neuroprosthetic interfaces *Crit. Rev. Biomed. Eng.* **44**
- [6] Struzyna L A *et al* 2017 Anatomically inspired three-dimensional micro-tissue engineered neural networks for nervous system reconstruction, modulation, and modeling *J. Vis. Exp.* **123** e55609
- [7] Friston K 2009 Causal modelling and brain connectivity in functional magnetic resonance imaging *PLoS Biol.* **7** 0220–5
- [8] Rykhlevskaia E, Gratton G and Fabiani M 2008 Combining structural and functional neuroimaging data for studying brain connectivity: a review *Psychophysiology* **45** 173–87
- [9] Astolfi L, Cincotti F, Mattia D, Babiloni C, Carducci F and Basilisco A 2005 Assessing cortical functional connectivity by linear inverse estimation and directed transfer function: simulations and application to real data *Clin. Neurophysiol.* **116** 920–32
- [10] Bastos A M and Schoffelen J-M 2015 A tutorial review of functional connectivity analysis methods and their interpretational pitfalls *Front. Syst. Neurosci.* **9** 175
- [11] Stevenson I H and Ko K P 2010 On the similarity of functional connectivity between neurons estimated across timescales *PLoS One* **5** e9206
- [12] Astolfi L *et al* 2004 Estimation of the effective and functional human cortical connectivity with structural equation modeling and directed transfer function applied to high-resolution EEG *Magn. Reson. Imaging* **22** 1457–70
- [13] Li K, Guo L, Nie J, Li G and Liu T 2009 Review of methods for functional brain connectivity detection using fMRI *Comput. Med. Imaging Graph.* **33** 131–9
- [14] Friston K J 2011 Functional and effective connectivity: a review *Brain Connect.* **1** 13–36
- [15] Friston K J 1994 Functional and effective connectivity in neuroimaging: a synthesis **2** 56–78
- [16] Babiloni F *et al* 2005 Estimation of the cortical functional connectivity with the multimodal integration of high-resolution EEG and fMRI data by directed transfer function *NeuroImage* **24** 118–31
- [17] Sakkalis V 2011 Review of advanced techniques for the estimation of brain connectivity measured with EEG/MEG *Comput. Biol. Med.* **41** 1110–7
- [18] Rubinov M and Sporns O 2010 Complex network measures of brain connectivity: uses and interpretations *NeuroImage* **52** 1059–69
- [19] Nguye J P *et al* 2015 Whole-brain calcium imaging with cellular resolution in freely behaving *Caenorhabditis elegans* *Proc. Natl Acad. Sci. USA* **113** E1074–81
- [20] Dombeck D A, Khabbaz A N, Collman F, Adelman T L and Tank D W 2007 Imaging large-scale neural activity with cellular resolution in awake, mobile mice *Neuron* **56** 43–57
- [21] Lütcke H, Gerhard F, Zenke F, Gerstner W and Helmchen F 2013 Inference of neuronal network spike dynamics and topology from calcium imaging data *Front. Neural Circuits* **7** 201
- [22] Cossart R, Ikegaya Y and Yuste R 2005 Calcium imaging of cortical networks dynamics *Cell Calcium* **37** 451–7
- [23] Grienberger C and Konnerth A 2012 Primer imaging calcium in neurons *Neuron Primer* **73** 862–85
- [24] Tang-Schomer M D, Davies P, Graziano D, Thurber A E and Kaplan D L 2014 Neural circuits with long-distance axon tracts for determining functional connectivity *J. Neurosci. Methods* **222** 82–90
- [25] Womelsdorf T *et al* 2007 Modulation of neuronal interactions through neuronal synchronization *Science* **316** 1609–13
- [26] Elsegai H, Shiells H, Thiel M and Schelter B 2015 Network inference in the presence of latent confounders: the role of instantaneous causalities *J. Neurosci. Methods* **245** 91–106
- [27] Fallani F D V, Corazzol M, Sternberg J R, Wyart C and Chavez M 2015 Hierarchy of neural organization in the embryonic spinal cord: granger-causality graph analysis of *in vivo* calcium imaging data *IEEE Eng. Med. Biol.* **23** 333–41
- [28] Buzsaki G 2006 *Rhythms of the Brain* (Oxford: Oxford University Press)
- [29] Dai J, Brooks D I and Sheinberg D L 2014 Optogenetic and electrical microstimulation systematically bias visuospatial choice in primates *Curr. Biol.* **24** 63–9
- [30] Patel T P, Man K, Firestein B L and Meaney D F 2015 Automated quantification of neuronal networks and single-cell calcium dynamics using calcium imaging *J. Neurosci. Methods* **243** 26–38
- [31] Horwitz B 2003 The elusive concept of brain connectivity *Sci. Direct* **19** 466–70
- [32] Netoff T I, Pecora L M and Schiff S J 2004 Analytical coupling detection in the presence of noise and nonlinearity *Phys. Rev. E* **69** 1–4
- [33] Liu X, Quan T, Zeng S and Lv X 2011 Identification of the direction of the neural network activation with a cellular resolution by fast two-photon imaging *J. Biomed. Opt.* **16** 080506
- [34] Bowman D 2013 A list of analytic expressions for instantaneous frequency determined via the hilbert transform 1–9 (<http://citeseerx.ist.psu.edu/viewdoc/download?doi=10.1.1.398.7463&rep=rep1&type=pdf>)
- [35] Allefeld C, Müller M and Kurths J 2007 Eigenvalue decomposition as a generalized synchronization cluster analysis *Int. J. Bifurc. Chaos* **17** 3493–7
- [36] Pita-Almenar J D, Yu D, Lu H-C and Beierlein M 2014 Mechanisms underlying desynchronization of cholinergic-evoked thalamic network activity *J. Neurosci.* **34** 14463–74
- [37] Wang Y, Toprani S, Tang Y, Vrabcic T and Durand D M 2014 Mechanism of highly synchronized bilateral hippocampal activity *Exp. Neurol.* **251** 101–11
- [38] Kaminski M J and Blinowska K J 1991 A new method of the description of the information flow in the brain structures *Biol. Cybern.* **65** 203–10
- [39] Estimate P V M and Kamin M 2004 Determination of EEG activity propagation: *IEE Trans. Biomed. Eng.* **51** 1501–10
- [40] Korzeniewska A, Kasicki S and Kamin M 1997 Information flow between hippocampus and related structures during various types of rat’s behavior *J. Neurosci. Methods* **73** 49–60
- [41] Mullen T 2010 Source information flow toolbox (SIFT) theoretical handbook and user manual *Swartz Cent. Comput. Neurosci.* 1–69 (<https://sccn.ucsd.edu/wiki/SIFT>)

- [42] Delorme A *et al* 2011 EEGLAB, SIFT, NFT, BCILAB, and ERICA: new tools for advanced EEG processing *Comput. Intell. Neurosci.* **2011** 130714
- [43] Belanger S, Oliveira Ferreira de Souza B, Casanova C and Lesage F L 2016 Correlation of hemodynamic and fluorescence signals under resting state conditions in mice's barrel field cortex *Neurosci. Lett.* **616** 177–81
- [44] Kramer M A 2013 An introduction to field analysis techniques: the power spectrum and coherence *2013 Short Course II: The Science of Large Data Sets: Spikes, Fields, and Voxels* (Washington DC: Society for Neuroscience) pp 18–25
- [45] Tibau E, Valencia M and Soriano J 2013 Identification of neuronal network properties from the spectral analysis of calcium imaging signals in neuronal cultures *Front. Neural Circuits* **7** 1–16
- [46] Kaiser A and Schreiber T 2002 Information transfer in continuous processes *Physica D* **166** 43–62
- [47] Goure B and Eggermont J J 2007 Evaluating information transfer between auditory cortical neurons *J. Neurophysiol.* **97** 2533–43
- [48] Orlandi J G, Stetter O, Soriano J, Geisel T and Battaglia D 2014 Transfer entropy reconstruction and labeling of neuronal connections from simulated calcium imaging *PLoS One* **9** e98842
- [49] Amigó J M, Monetti R, Tort-Colet N and Sanchez-Vives M V 2015 Infragranular layers lead information flow during slow oscillations according to information directionality indicators *J. Comput. Neurosci.* **39** 53–62
- [50] Lizier J T 2014 JIDT: an information-theoretic toolkit for studying the dynamics of complex systems *Front. Robot. AI* **1** 11
- [51] Akam T and Kullmann D M 2014 Oscillatory multiplexing of population codes for selective communication in the mammalian brain *Nat. Rev. Neurosci.* **15** 111–22
- [52] Rutishauser U, Ross I B, Mamelak A N and Schuman E M 2010 Human memory strength is predicted by theta-frequency phase-locking of single neurons *Nature* **464** 903–7
- [53] Benchenane K *et al* 2010 Coherent theta oscillations and reorganization of spike timing in the hippocampal-prefrontal network upon learning *Neuron* **66** 921–36
- [54] Chen H-C I, Wolf J and Smith D 2017 Multichannel activity propagation across an engineered axon network *J. Neural Eng.* **14** 026016
- [55] Shein M, Volman V, Raichman N, Hanein Y and Ben-Jacob E 2008 Management of synchronized network activity by highly active neurons *Phys. Biol.* **5** 036008
- [56] Lonardoni D, Amin H, Di Marco S, Maccione A, Berdondini L and Nieuws T 2017 Recurrently connected and localized neuronal communities initiate coordinated spontaneous activity in neuronal networks *PLoS Comput. Biol.* **13** 1–27
- [57] Chiappalone M, Vato A, Berdondini L, Koudelka-Hep M and Martinoia S 2007 Network dynamics and synchronous activity in cultured cortical neurons *Int. J. Neural Syst.* **17** 87–103
- [58] Cappaert N L M, Lopes Da Silva F H and Wadman W J 2009 Spatio-temporal dynamics of theta oscillations in hippocampal-entorhinal slices *Hippocampus* **19** 1065–77
- [59] Poli D, Pastore V P, Martinoia S and Massobrio P 2016 From functional to structural connectivity using partial correlation in neuronal assemblies *J. Neural Eng.* **13** 026023
- [60] Zhuang P, Sun A X, An J, Chua C K and Chew S Y 2018 3D neural tissue models: from spheroids to bioprinting *Biomaterials* **154** 113–33
- [61] Hopkins A M, DeSimone E, Chwalek K and Kaplan D L 2015 3D *in vitro* modeling of the central nervous system *Prog. Neurobiol.* **125** 1–25
- [62] Schmidt C E and Leach J B 2003 Neural tissue engineering: strategies for repair and regeneration *Annu. Rev. Biomed. Eng.* **5** 293–347
- [63] Fennema E, Rivron N, Rouwkema J, van Blitterswijk C and de Boer J 2013 Spheroid culture as a tool for creating 3D complex tissues *Trends Biotechnol.* **31** 108–15
- [64] Han C, Takayama S and Park J 2015 Formation and manipulation of cell spheroids using a density adjusted PEG/DEX aqueous two phase system *Sci. Rep.* **5** 11891
- [65] Dingle Y-T L *et al* 2015 Three-dimensional neural spheroid culture: an *in vitro* model for cortical studies *Tissue Eng. C* **21** 1274–83
- [66] Qian X *et al* 2016 Brain-region-specific organoids using mini-bioreactors for modeling ZIKV exposure *Cell* **165** 1238–54
- [67] Lancaster M A and Knoblich J A 2014 Generation of cerebral organoids from human pluripotent stem cells *Nat. Protocols* **9** 2329
- [68] Lancaster M A *et al* 2013 Cerebral organoids model human brain development and microcephaly *Nature* **501** 373
- [69] Gao S *et al* 2014 Differentiation of human adipose-derived stem cells into neuron-like cells which are compatible with photocurable three-dimensional scaffolds *Tissue Eng. A* **20** 1271–84
- [70] Hopkins A M *et al* 2013 Silk hydrogels as soft substrates for neural tissue engineering *Adv. Funct. Mater.* **23** 5140–9
- [71] Xu Y, Zhang Z, Chen X, Li R, Li D and Feng S 2016 A silk fibroin/collagen nerve scaffold seeded with a co-culture of schwann cells and adipose-derived stem cells for sciatic nerve regeneration *PLoS One* **11** e0147184
- [72] van Duinen V, Trietsch S J, Joore J, Vulto P and Hankemeier T 2015 Microfluidic 3D cell culture: from tools to tissue models *Curr. Opin. Biotechnol.* **35** 118–26
- [73] Mandrycky C, Wang Z, Kim K and Kim D-H 2016 3D bioprinting for engineering complex tissues *Biotechnol. Adv.* **34** 422–34